Research Square

Preprints are preliminary reports that have not undergone peer review.
They should not be considered conclusive, used to inform clinical practice,
or referenced by the media as validated information.

Harmonic Chaos

Michele Bonnin

michele.bonnin@polito.it

Politecnico di Torino

Kailing Song

Politecnico di Torino

Fabio Traversa

Memcomputing (United States)

Fabrizio Bonani

Politecnico di Torino

Research Article

Keywords: stochastic differential equations, Karhunen–Lo`eve expansion, harmonic balance, polynomial chaos, stochastic Duffing oscillator, Ornstein–Uhlenbeck process

Posted Date: November 12th, 2026

DOI: https://doi.org/10.21203/rs.3.rs-11409714/v1

License: This work is licensed under a Creative Commons Attribution 4.0 International License.
Read Full License

Additional Declarations: No competing interests reported.

Harmonic Chaos

Michele Bonnin[1*], Kailing Song[1], Fabio Traversa[2], Fabrizio Bonani[1]

[1]Department of Electronics and Telecommunications, Politecnico di Torino, Turin, Italy.
[2]Memcomputing Inc., La Jolla, CA, USA.

*Corresponding author(s). E-mail(s): michele.bonnin@polito.it;
Contributing authors: kailing.song@polito.it; ftraversa@memcpu.com;
fabrizio.bonani@polito.it;

Abstract

We introduce Harmonic Chaos, a semi-analytical method for computing stationary statistics of stochastic differential equations driven by Gaussian white noise. The method is based on the combined application of the Karhunen-Loève expansion of the Wiener process, harmonic balance, and polynomial chaos, and permits to transform stochastic differential equations into systems of algebraic equations, with deterministic coefficients as unknowns. The procedure can be summarized as follows: on a finite time interval, the stochastic differential equation is transformed into a family of periodically forced ordinary differential equations parametrized by independent Gaussian variables by means of a truncated Karhunen-Loève expansion applied to the Wiener process feeding the stochastic system. This enables use of harmonic balance for their solution. The amplitudes of the harmonics depend on the random variables, in turn expanded through Hermite polynomial chaos. Applying a coupled temporal-stochastic Galerkin projection, we obtain a system of algebraic equations for the coefficients of the polynomial chaos representation. Once the algebraic system has been solved, stationary statistical moments can be calculated directly, while probability density functions can be obtained by sampling the resulting representation without repeatedly solving the dynamical equations. The method is first validated applying it to the Ornstein-Uhlenbeck process, for which the Harmonic Chaos equations can be solved analytically. The application of the method to nonlinear problems is demonstrated by considering a stochastic Duffing oscillator. We show that, by exploiting the symmetries of the system, a reduced spectral representation can be found that allows for a computationally tractable numerical implementation. The resulting stationary marginal distributions of displacement and velocity show good agreement with the corresponding analytical distributions.

Keywords: stochastic differential equations, Karhunen–Loève expansion, harmonic balance, polynomial chaos, stochastic Duffing oscillator, Ornstein–Uhlenbeck process

1 Introduction

Stochastic differential equations (SDEs) provide a mathematical framework for modeling dynamical systems subject to random fluctuations, with applications ranging from noisy electronic oscillators and circuits [1–4] to mechanical systems and structural vibrations [5–8], and statistical physics [9–11]. In many of these applications, the relevant quantities are not individual trajectories, but rather the stationary statistical properties of the response, including moments, correlation functions, probability density functions, and probabilities of exceeding critical thresholds. How

determining these quantities remains a challenging problem, particularly for nonlinear systems, where analytical solutions are rarely available.

Several approaches have been developed to investigate the statistical behavior of stochastic dynamical systems, each with its own pros and cons. Monte Carlo methods, based on the numerical integration of large ensembles of stochastic trajectories, are general and broadly applicable, but their statistical convergence is slow, and accurate estimation of distribution tails or rare events may require a very large number of realizations [12, 13]. Numerical solutions of the Fokker-Planck equation, obtained for example through finite differences or finite elements, provide direct access to the probability density function, but their computational cost increases rapidly with the dimension of the state space [14, 15]. Moment-closure and statistical-linearization techniques offer computationally inexpensive alternatives, although their accuracy can be difficult to control for strongly nonlinear systems and markedly non-Gaussian distributions [16, 17]. Spectral stochastic methods, particularly those based on Wiener chaos and generalized polynomial chaos, describe the dependence of the response on random variables through expansions in orthogonal polynomials [18, 19]. However, their application to long-time stochastic dynamics may require increasingly rich stochastic representations to maintain accuracy, making the computation of stationary statistics demanding [20, 21].

Frequency-domain methods provide a complementary approach to the analysis of dynamical systems. Harmonic balance, in particular, transforms the computation of periodic responses into an algebraic problem by representing the solution through a truncated Fourier series, thereby avoiding direct time integration [22–24]. Harmonic balance has also been combined with polynomial chaos and other stochastic spectral techniques to investigate periodically driven systems with uncertain parameters [25, 26]. These approaches exploit the complementary roles of Fourier expansions in describing temporal variations, and of polynomial chaos in representing stochastic dependence. However, the direct application of conventional harmonic balance to SDEs driven by Gaussian white noise is not straightforward, since white-noise realizations are neither smooth nor periodic.

Harmonic Chaos (HC) combines these ideas to construct a semi-analytical method for computing stationary statistics of SDEs driven by additive Gaussian white noise. The key observation is that the Karhunen-Loève (KL) expansion of the Wiener process on a finite interval $[0, T]$ involves odd multiples of a fundamental frequency. Consequently, the derivative of its truncated representation defines a smooth, finite-dimensional approximation of white noise that admits a periodic extension with period $4T$. For each realization of the independent Gaussian KL coefficients, the SDE is thus transformed into a deterministic differential equation with periodic forcing, allowing harmonic balance to be applied. The resulting harmonic amplitudes depend on the Gaussian random variables defining the excitation and are therefore themselves random variables. The dependence of the harmonic amplitudes on the KL coefficients is represented through Hermite polynomial chaos, and a coupled temporal-stochastic Galerkin projection determines all expansion coefficients simultaneously, without solving separate harmonic-balance problems for individual realizations of the excitation. Once these coefficients are available, statistical moments can be calculated algebraically, while probability densities and other statistical quantities can be estimated by sampling the resulting spectral representation, without further integration of the underlying SDE.

Stationary statistics are obtained by evaluating the HC representation at $t = T$, with T chosen sufficiently large compared with the characteristic relaxation time of the system. It is important to emphasize that the periodicity introduced by the KL representation is a computational tool rather than a property of the original stochastic process. The KL expansion retains its probabilistic interpretation only on $[0, T]$, and only the restriction of the corresponding harmonic-balance solution to this interval is used to approximate the stochastic response. Accordingly, the present formulation is intended for stationary statistical analysis rather than the reconstruction of transient solutions associated with prescribed initial conditions. Although the analysis presented here is restricted to additive Gaussian noise for simplicity, the HC framework can also be extended to multiplicative noise, since the product of a periodic state-dependent coefficient and the periodic forcing obtained from the truncated KL expansion remains periodic.

The main contributions of this work are the following:

- A HC formulation is developed for systems of SDEs driven by additive Gaussian noise, including correlated Wiener sources. The coupled temporal-stochastic Galerkin equations are derived, together with the Hermite coupling coefficients required for the algebraic projection of polynomial nonlinearities.
- The method is applied to the Ornstein-Uhlenbeck process, for which the HC equations are solved entirely analytically. Closed-form expressions are obtained for the stochastic response and its principal statistical quantities, including the expected value, variance, and autocovariance. These expressions are shown analytically to recover the corresponding classical stationary results in the appropriate limits.
- The applicability of HC to nonlinear systems is demonstrated using a stochastic Duffing oscillator. Half-wave and stochastic parity symmetries are exploited to reduce the temporal and polynomial-chaos representations. In particular, a third-order Hermite expansion is identified as the lowest-order approximation capable of representing a non-Gaussian displacement distribution. The stationary marginal densities of displacement and velocity obtained from HC are compared with the corresponding analytical distributions.
- The computational implementation combines symmetry reduction, a sparse Hermite basis, and a matrix-free Newton-Krylov solver to mitigate the combinatorial growth of the coupled algebraic system with the number of KL modes. This approach enables the numerical solution of a high-dimensional Galerkin system while retaining the nonlinear stochastic dependence of the response.

The paper is organized as follows. Section 2 reviews the mathematical background of the Karhunen-Loève expansion, harmonic balance, and polynomial chaos. Section 3 develops the HC formulation, while Section 4 describes how stationary statistics are evaluated and sampled from the resulting spectral representation. Section 5 presents the analytical treatment of the Ornstein-Uhlenbeck process and the numerical application to the stochastic Duffing oscillator. Section 6 summarizes the main results and conclusions. The properties of the truncated KL representation and the algebra of Hermite coupling coefficients are summarized in Appendix A and Appendix B, respectively.

2 Mathematical background

This section introduces the three mathematical tools on which the Harmonic Chaos method is based: the Karhunen-Loève expansion, harmonic balance, and polynomial chaos. Only the results required for the subsequent development are recalled, with the aim of establishing the notation and making the presentation self-contained. The coupling among these three ingredients, which constitutes the proposed Harmonic Chaos formulation, is developed in Section 3.

2.1 Karhunen-Loève expansion

Let $(\Omega, \mathcal{F}, \mathbb{P})$ be a probability space, and let $X : [0,T] \times \Omega \to \mathbb{R}$ be a real-valued, mean-square continuous, second-order Gaussian stochastic process. Here, Gaussian means that every finite collection $X(t_1), \ldots, X(t_q)$ is jointly Gaussian, whereas second order requires that

$$\mathbb{E}[X^2(t)] < +\infty, \qquad t \in [0,T].$$

The expectation function of X is

$$m_X(t) = \mathbb{E}[X(t)], \tag{1}$$

while the covariance function is

$$C_X(t,s) = \mathbb{E}\left[\big(X(t) - m_X(t)\big)\big(X(s) - m_X(s)\big)\right] \tag{2}$$

The covariance function defines the self-adjoint, positive semidefinite, and compact integral operator

$$\mathcal{C}_X \phi(t) = \int_0^T C_X(t,s)\phi(s)\,\mathrm{d}s, \quad \phi \in L^2([0,T]). \tag{3}$$

Eigenfunctions $e_n(t)$ and eigenvalues λ_n of $\mathcal{C}_X$ satisfy

$$\int_0^T C_X(t,s)e_n(s)\,\mathrm{d}s = \lambda_n e_n(t), \tag{4}$$

with

$$\int_0^T e_n(t)e_j(t)\,\mathrm{d}t = \delta_{nj}. \tag{5}$$

The eigenvalues are real and non-negative and can be ordered as

$$\lambda_1 \geq \lambda_2 \geq \cdots \geq 0. \tag{6}$$

The Karhunen-Loève representation of the process is [27, 28]

$$X(t) = m_X(t) + \sum_{n=1}^{+\infty} \sqrt{\lambda_n}\,\zeta_n e_n(t), \tag{7}$$

where, for each $\lambda_n > 0$, the random coefficients are given by

$$\zeta_n = \frac{1}{\sqrt{\lambda_n}} \int_0^T \big(X(t) - m_X(t)\big) e_n(t)\,\mathrm{d}t. \tag{8}$$

They have zero expectation and unit covariance:

$$\mathbb{E}[\zeta_n] = 0, \qquad \mathbb{E}[\zeta_n \zeta_j] = \delta_{nj}. \tag{9}$$

Since $X(t)$ is Gaussian, the coefficients are jointly Gaussian. Consequently, their uncorrelatedness implies independence, and

$$\zeta_n \overset{\text{i.i.d.}}{\sim} \mathcal{N}(0,1). \tag{10}$$

Under the usual regularity assumptions on the covariance function, the series in (7) converges in the mean-square sense. In particular,

$$\lim_{N\to+\infty} \mathbb{E}\left[\int_0^T |X(t) - X_N(t)|^2\,\mathrm{d}t\right] = 0, \tag{11}$$

where

$$X_N(t) = m_X(t) + \sum_{n=1}^{N} \sqrt{\lambda_n}\,\zeta_n e_n(t) \tag{12}$$

is the N-term KL approximation. Its integrated mean-square truncation error is

$$\mathbb{E}\left[\int_0^T |X(t) - X_N(t)|^2\,\mathrm{d}t\right] = \sum_{n=N+1}^{+\infty} \lambda_n. \tag{13}$$

The KL expansion is optimal in the mean-square sense: among all representations based on N deterministic orthonormal functions, it minimizes the integrated truncation error [29].

We now specialize the expansion to a standard Wiener process $W(t)$. Its expectation and covariance functions are

$$\mathbb{E}[W(t)] = 0, \qquad C_W(t,s) = \min(t,s). \tag{14}$$

The eigenvalue problem associated with this covariance kernel is

$$\int_0^T \min(t,s) e_n(s)\,\mathrm{d}s = \lambda_n e_n(t). \tag{15}$$

Its eigenvalues and normalized eigenfunctions are

$$\lambda_n = \frac{T^2}{\left(n-\frac{1}{2}\right)^2 \pi^2}, \tag{16a}$$

$$e_n(t) = \sqrt{\frac{2}{T}} \sin\left[\left(n-\frac{1}{2}\right)\frac{\pi}{T}t\right]. \tag{16b}$$

Introducing the fundamental frequency

$$\omega_0 = \frac{\pi}{2T}, \tag{17}$$

the KL representation of the Wiener process on $[0,T]$ can be written as

$$W(t) = \sqrt{2T} \sum_{n=1}^{+\infty} \zeta_n \frac{\sin\left[(2n-1)\omega_0 t\right]}{(2n-1)\pi/2}. \tag{18}$$

Retaining only the first N terms gives the finite-dimensional approximation

$$W_N(t) = \sqrt{2T} \sum_{n=1}^{N} \zeta_n \frac{\sin\left[(2n-1)\omega_0 t\right]}{(2n-1)\pi/2}. \tag{19}$$

The left panel of Fig. 1 illustrates the effect of truncating the KL expansion. As the number of retained modes increases, finer temporal fluctuations become visible, and the realizations exhibit the characteristic irregular behavior of Wiener paths. The right panel compares two realizations of the Wiener process generated using different methods, one based on independent Gaussian increments and the other on the KL expansion.

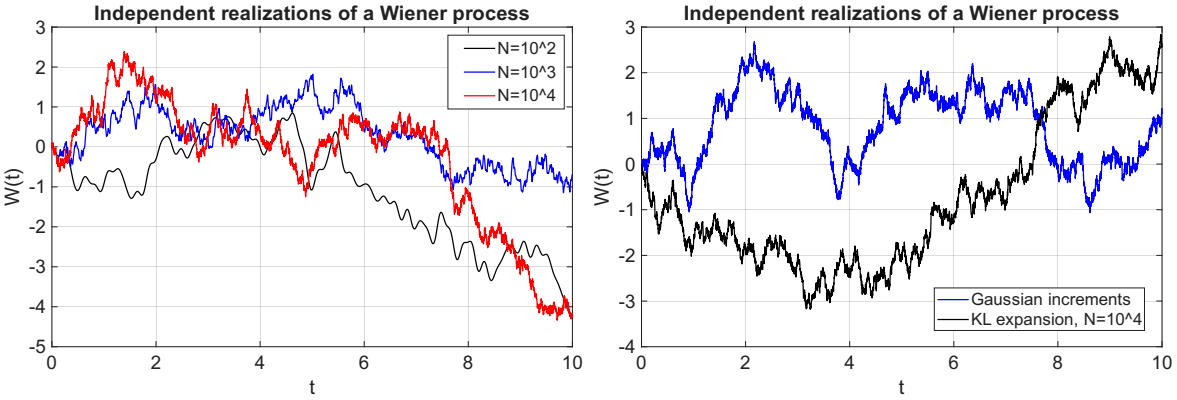


Fig. 1: Left: Three KL realizations of the Wiener process with a different number N of harmonics. Right: Comparison between two realizations of the Wiener process, obtained using Gaussian increments and a KL representation of the driving Wiener process, respectively.

The two realizations show the same qualitative features.

For fixed N, $W_N(t)$ is a smooth Gaussian process. It can therefore be differentiated using the ordinary rules of calculus, giving

$$\eta_N(t) \equiv \frac{\mathrm{d}W_N(t)}{\mathrm{d}t} = \sqrt{\frac{2}{T}} \sum_{n=1}^{N} \zeta_n \cos\left[(2n-1)\omega_0 t\right]. \tag{20}$$

The process $\eta_N(t)$ is a smooth, finite-dimensional approximation of Gaussian white noise. Its covariance and its convergence in the generalized sense are discussed in Appendix A.

All the frequencies appearing in (19) and (20) are odd multiples of ω_0. Therefore, $W_N(t)$ and $\eta_N(t)$ admit sample-wise periodic extensions with fundamental period

$$\mathcal{T}_0 = \frac{2\pi}{\omega_0} = 4T. \tag{21}$$

This periodicity is a consequence of the trigonometric representation and will be exploited to apply harmonic balance. It must not, however, be attributed to the original Wiener process. The KL representation has stochastic meaning only on the interval $[0, T]$; outside this interval, the periodic continuation is an artificial computational extension and does not preserve the probabilistic properties of Brownian motion.

Consequently, only the restriction to $[0, T]$ of the solution obtained from the periodically extended forcing is interpreted as an approximation of the original stochastic system.

2.2 Harmonic balance

Harmonic balance is a frequency-domain method for computing periodic solutions of nonlinear differential equations [30, 31]. Consider the d-dimensional system

$$\frac{\mathrm{d}\boldsymbol{x}}{\mathrm{d}t} = \boldsymbol{f}(\boldsymbol{x}, t), \qquad \boldsymbol{x}(t) \in \mathbb{R}^d, \tag{22}$$

where the vector field is periodic in time with period $\mathcal{T}_0$ and $\omega_0 = 2\pi/\mathcal{T}_0$:

$$\boldsymbol{f}(\boldsymbol{x}, t + \mathcal{T}_0) = \boldsymbol{f}(\boldsymbol{x}, t). \tag{23}$$

Assume that the system admits a periodic solution with the same period as the forcing:

$$\boldsymbol{x}(t + \mathcal{T}_0) = \boldsymbol{x}(t). \tag{24}$$

The harmonic-balance approximation is obtained by truncating the Fourier representation of the solution at harmonic order H:

$$\boldsymbol{x}_H(t) = \boldsymbol{A}_0 + \sum_{k=1}^{H} \left[\boldsymbol{A}_k \cos(k\omega_0 t) + \boldsymbol{B}_k \sin(k\omega_0 t)\right]. \tag{25}$$

Here, $\boldsymbol{A}_0, \boldsymbol{A}_k, \boldsymbol{B}_k \in \mathbb{R}^d$ are the unknown vector harmonic coefficients. Thus, each component of the state has its own Fourier representation,

while all components share the same fundamental frequency.

The time derivative of the approximation is

$$\frac{\mathrm{d}\boldsymbol{x}_H}{\mathrm{d}t} = \sum_{k=1}^{H} k\omega_0 \left[\boldsymbol{B}_k \cos(k\omega_0 t) - \boldsymbol{A}_k \sin(k\omega_0 t)\right]. \tag{26}$$

The nonlinear vector field evaluated along the approximate solution is projected onto the same Fourier basis:

$$\boldsymbol{f}\big(\boldsymbol{x}_H(t), t\big) \simeq \boldsymbol{F}_0 + \sum_{k=1}^{H} \Big[\boldsymbol{F}_k^{(c)} \cos(k\omega_0 t) + \boldsymbol{F}_k^{(s)} \sin(k\omega_0 t)\Big]. \tag{27}$$

The Fourier coefficients of the nonlinear vector field are

$$\boldsymbol{F}_0 = \frac{1}{\mathcal{T}_0} \int_0^{\mathcal{T}_0} \boldsymbol{f}\big(\boldsymbol{x}_H(t), t\big)\, \mathrm{d}t, \tag{28}$$

$$\boldsymbol{F}_k^{(c)} = \frac{2}{\mathcal{T}_0} \int_0^{\mathcal{T}_0} \boldsymbol{f}\big(\boldsymbol{x}_H(t), t\big) \cos(k\omega_0 t)\, \mathrm{d}t, \tag{29}$$

$$\boldsymbol{F}_k^{(s)} = \frac{2}{\mathcal{T}_0} \int_0^{\mathcal{T}_0} \boldsymbol{f}\big(\boldsymbol{x}_H(t), t\big) \sin(k\omega_0 t)\, \mathrm{d}t, \tag{30}$$

for $k = 1, \ldots, H$. Through $\boldsymbol{x}_H(t)$, all these Fourier coefficients depend, in general, on the complete set $\boldsymbol{A}_0, \boldsymbol{A}_1, \boldsymbol{B}_1, \ldots, \boldsymbol{A}_H, \boldsymbol{B}_H$. In particular, the nonlinearities couple different state variables and different temporal harmonics.

Substituting the two truncated Fourier representations into the differential equation and equating corresponding Fourier coefficients, or equivalently imposing a temporal Galerkin projection of the residual, gives

$$\boldsymbol{F}_0 = \boldsymbol{0}, \tag{31}$$

$$\boldsymbol{F}_k^{(c)} - k\omega_0 \boldsymbol{B}_k = \boldsymbol{0}, \qquad k = 1, \ldots, H, \tag{32}$$

$$\boldsymbol{F}_k^{(s)} + k\omega_0 \boldsymbol{A}_k = \boldsymbol{0}, \qquad k = 1, \ldots, H. \tag{33}$$

These equations form a nonlinear algebraic system of $d(2H + 1)$ scalar equations for the same number of unknown harmonic coefficients. The integrals defining the Fourier coefficients are temporal projections over one period; when the period originates from a KL representation, they must not be interpreted as statistical time averages.

For polynomial nonlinearities, the coefficients $\boldsymbol{F}_k^{(c)}$ and $\boldsymbol{F}_k^{(s)}$ can be evaluated analytically by performing algebraic operations on the Fourier series. For a general nonlinear vector field, they can be evaluated numerically. A common procedure is the alternating frequency-time method: the harmonic coefficients are first transformed to a set of time-domain samples, the nonlinear function is evaluated pointwise, and its Fourier coefficients are then recovered using a discrete Fourier transform [22].

Truncating the solution at harmonic order H does not imply that the nonlinear vector field contains only the first H harmonics. Nonlinearities generally generate higher-order harmonic components. The truncated Fourier representation of the nonlinear vector field must therefore be interpreted as its projection onto the retained Fourier space. The neglected components constitute the harmonic truncation error.

The decay rate of the Fourier coefficients depends on the temporal regularity of the periodic solution. A finite degree of differentiability generally leads to algebraic convergence, whereas analytic periodic solutions exhibit exponential decay of their Fourier coefficients. Under the additional assumption that the periodic solution is isolated and that the corresponding linearized operator is nonsingular, the harmonic-balance approximation is expected to converge to that solution as H increases. The convergence rate decreases when the solution has limited regularity or contains sharp temporal variations. Consequently, the harmonic order must be increased until the quantities of interest become insensitive to further enrichment of the Fourier basis.

Finally, the harmonic-balance equations determine periodic solutions but do not, by themselves, establish their stability or uniqueness. Nonlinear systems may possess multiple periodic solutions with the prescribed period $\mathcal{T}_0$, as well as subharmonic or quasiperiodic responses. Different periodic solutions can be obtained by solving the nonlinear algebraic system with different initial guesses for the harmonic coefficients. In the present formulation, only solutions having the prescribed period $\mathcal{T}_0$ are sought. Their stability can be assessed separately, for example through Floquet analysis [23].

2.3 Polynomial chaos expansion

Polynomial chaos is a method for representing square-integrable functions of a finite set of random variables as an expansion in terms of polynomial functions of those same variables [29, 32]. It provides a spectral description of the dependence on the random variables, in which the expansion coefficients are deterministic and the stochastic dependence is described by the polynomial basis functions. The polynomial basis is chosen according to the probability distribution of the random variables, so that the basis functions are orthogonal with respect to the corresponding probability measure. Under suitable assumptions, the resulting expansion converges in the mean-square sense. In the present work, the random variables arise from the Karhunen-Loève representation of the Wiener process and are independent standard Gaussian variables; therefore, the appropriate polynomial-chaos basis is constructed from Hermite polynomials.

Let $\boldsymbol{\zeta} = [\zeta_1, \ldots, \zeta_r]^\mathsf{T} : \Omega \to \Gamma \subseteq \mathbb{R}^r$, be the vector of random variables. Its probability distribution on Γ is denoted by μ. A function $u : \Gamma \to \mathbb{R}$ belongs to $L^2_\mu(\Gamma)$ if

$$\mathbb{E}\left[u^2(\boldsymbol{\zeta})\right] = \int_\Gamma u^2(\boldsymbol{\zeta})\,\mathrm{d}\mu(\boldsymbol{\zeta}) < +\infty. \tag{34}$$

For two real-valued functions $u, v \in L^2_\mu(\Gamma)$, define the stochastic inner product

$$\mathbb{E}\left[u(\boldsymbol{\zeta})v(\boldsymbol{\zeta})\right] = \int_\Gamma u(\boldsymbol{\zeta})v(\boldsymbol{\zeta})\,\mathrm{d}\mu(\boldsymbol{\zeta}). \tag{35}$$

Assume that the polynomials are dense in $L^2_\mu(\Gamma)$. This ensures that the polynomial basis is complete in $L^2_\mu(\Gamma)$, so that any square-integrable function of $\boldsymbol{\zeta}$ can be approximated arbitrarily well, in the mean-square sense, by increasing the polynomial order. An orthonormal polynomial basis can then be constructed and indexed by the multi-indices

$$\boldsymbol{\alpha} = (\alpha_1, \ldots, \alpha_r) \in \mathbb{N}_0^r, \quad \mathbb{N}_0 = \{0, 1, 2, \ldots\}. \tag{36}$$

The total degree of a multi-index is defined as

$$|\boldsymbol{\alpha}| = \sum_{j=1}^{r} \alpha_j. \tag{37}$$

Denoting the multivariate polynomial associated with $\boldsymbol{\alpha}$ by $\Psi_{\boldsymbol{\alpha}}(\boldsymbol{\zeta})$, orthonormality means that

$$\mathbb{E}\left[\Psi_{\boldsymbol{\alpha}}(\boldsymbol{\zeta})\Psi_{\boldsymbol{\beta}}(\boldsymbol{\zeta})\right] = \delta_{\boldsymbol{\alpha}\boldsymbol{\beta}}. \tag{38}$$

Any square-integrable vector-valued function $\boldsymbol{Y} : \Gamma \to \mathbb{R}^d$ can therefore be represented component-wise as

$$\boldsymbol{Y}(\boldsymbol{\zeta}) = \sum_{\boldsymbol{\alpha} \in \mathbb{N}_0^r} \boldsymbol{y}_{\boldsymbol{\alpha}} \Psi_{\boldsymbol{\alpha}}(\boldsymbol{\zeta}), \qquad \boldsymbol{y}_{\boldsymbol{\alpha}} \in \mathbb{R}^d, \tag{39}$$

where the deterministic polynomial-chaos coefficients are obtained by orthogonal projection:

$$\boldsymbol{y}_{\boldsymbol{\alpha}} = \mathbb{E}\left[\boldsymbol{Y}(\boldsymbol{\zeta})\Psi_{\boldsymbol{\alpha}}(\boldsymbol{\zeta})\right]. \tag{40}$$

The deterministic coefficients quantify the contribution of the different polynomial modes to the dependence of $\boldsymbol{Y}$ on the random variables. For an orthonormal polynomial basis, the mean of the expansion is given by the zero-order coefficient,

$$\mathbb{E}[\boldsymbol{Y}] = \boldsymbol{y}_{\boldsymbol{0}}, \tag{41}$$

whereas the covariance matrix is

$$\mathrm{Cov}[\boldsymbol{Y}] = \sum_{\boldsymbol{\alpha} \neq \boldsymbol{0}} \boldsymbol{y}_{\boldsymbol{\alpha}} \boldsymbol{y}_{\boldsymbol{\alpha}}^T. \tag{42}$$

The basis functions $\Psi_{\boldsymbol{\alpha}}$ are scalar, whereas the coefficients $\boldsymbol{y}_{\boldsymbol{\alpha}}$ carry the vector structure of $\boldsymbol{Y}$. The scalar expansion is recovered by setting $d = 1$, and the series converges in the mean-square sense.

The appropriate family of orthogonal polynomials depends on the probability distribution of $\boldsymbol{\zeta}$. In the Gaussian case considered here, the random vector satisfies $\boldsymbol{\zeta} \sim \mathcal{N}(\boldsymbol{0}, \boldsymbol{I}_r)$, with joint probability density

$$\rho_r(\boldsymbol{\zeta}) = \frac{1}{(2\pi)^{r/2}} \exp\left(-\frac{1}{2}\boldsymbol{\zeta}^T\boldsymbol{\zeta}\right). \tag{43}$$

For a standard Gaussian random variable, the corresponding orthogonal polynomials are the probabilists' Hermite polynomials ($p \in \mathbb{N}_0$)

$$\mathrm{He}_p(\zeta) = (-1)^p \exp\left(\frac{\zeta^2}{2}\right) \frac{d^p}{d\zeta^p} \exp\left(-\frac{\zeta^2}{2}\right), \tag{44}$$

which satisfy

$$\mathbb{E}\left[\mathrm{He}_p(\zeta)\,\mathrm{He}_q(\zeta)\right] = p!\,\delta_{pq}. \tag{45}$$

The normalized Hermite polynomials are therefore defined as

$$\psi_p(\zeta) = \frac{\mathrm{He}_p(\zeta)}{\sqrt{p!}}, \tag{46}$$

so that

$$\mathbb{E}\left[\psi_p(\zeta)\psi_q(\zeta)\right] = \delta_{pq}. \tag{47}$$

The multivariate Hermite polynomials are constructed as

$$\Psi_{\boldsymbol{\alpha}}(\boldsymbol{\zeta}) = \prod_{j=1}^{r} \psi_{\alpha_j}(\zeta_j). \tag{48}$$

Since the components of $\boldsymbol{\zeta}$ are independent,

$$\mathbb{E}\left[\Psi_{\boldsymbol{\alpha}}(\boldsymbol{\zeta})\Psi_{\boldsymbol{\beta}}(\boldsymbol{\zeta})\right] = \prod_{j=1}^{r} \mathbb{E}\left[\psi_{\alpha_j}(\zeta_j)\psi_{\beta_j}(\zeta_j)\right] = \delta_{\boldsymbol{\alpha}\boldsymbol{\beta}}. \tag{49}$$

The zero-order polynomial is

$$\Psi_{\mathbf{0}}(\boldsymbol{\zeta}) = 1, \tag{50}$$

and all higher-order basis functions have zero expectation,

$$\mathbb{E}\left[\Psi_{\boldsymbol{\alpha}}(\boldsymbol{\zeta})\right] = 0, \qquad \boldsymbol{\alpha} \neq \mathbf{0}. \tag{51}$$

Moreover, since $\psi_1(\zeta) = \zeta$, each Gaussian variable ζ_j corresponds to the first-order multivariate Hermite polynomial $\Psi_{\boldsymbol{\alpha}}(\boldsymbol{\zeta}) = \zeta_j$, where $\alpha_j = 1$ and $\alpha_i = 0$ for $i \neq j$. The polynomial degree of $\Psi_{\boldsymbol{\alpha}}$ is $|\boldsymbol{\alpha}|$.

Explicit expressions for the first normalized Hermite polynomials and an example of the construction of a multivariate basis function are provided in Appendix B.

For numerical computations, the infinite polynomial-chaos expansion must be truncated. A commonly used choice is the total-degree index set

$$\mathcal{A}_{r,P} = \left\{\boldsymbol{\alpha} \in \mathbb{N}_0^r : |\boldsymbol{\alpha}| \leq P\right\}, \tag{52}$$

where P is the maximum retained total degree. Thus, the truncation retains all polynomial modes with total degree not exceeding P, including mixed terms that describe interactions among different random variables. The corresponding polynomial-chaos approximation is

$$\boldsymbol{Y}_P(\boldsymbol{\zeta}) = \sum_{\boldsymbol{\alpha} \in \mathcal{A}_{r,P}} \boldsymbol{y}_{\boldsymbol{\alpha}} \Psi_{\boldsymbol{\alpha}}(\boldsymbol{\zeta}). \tag{53}$$

Again, the scalar case follows by setting $d = 1$. The number of retained basis functions is

$$K = |\mathcal{A}_{r,P}| = \binom{r+P}{P}. \tag{54}$$

By orthonormality, the mean-square truncation error for a scalar square-integrable function is

$$\mathbb{E}\left[\left|Y(\boldsymbol{\zeta}) - Y_P(\boldsymbol{\zeta})\right|^2\right] = \sum_{\boldsymbol{\alpha} \notin \mathcal{A}_{r,P}} y_{\boldsymbol{\alpha}}^2. \tag{55}$$

Consequently, for fixed stochastic dimension r,

$$\lim_{P \to +\infty} \mathbb{E}\left[\left|Y(\boldsymbol{\zeta}) - Y_P(\boldsymbol{\zeta})\right|^2\right] = 0. \tag{56}$$

The convergence rate depends on the regularity of the dependence of Y on the random variables, whereas the number of retained coefficients grows combinatorially with both r and P.

3 Harmonic Chaos method for systems of stochastic differential equations

The mathematical tools introduced in Section 2 are now combined to construct the Harmonic Chaos (HC) approximation of a system of stochastic differential equations. The present formulation is restricted to additive Gaussian noise.

3.1 Problem formulation

Consider the system of autonomous stochastic differential equations

$$\mathrm{d}\boldsymbol{x}(t) = \boldsymbol{f}\big(\boldsymbol{x}(t)\big)\,\mathrm{d}t + \boldsymbol{G}\,\mathrm{d}\boldsymbol{W}(t), \qquad \boldsymbol{x}(t) \in \mathbb{R}^d, \tag{57}$$

where $\boldsymbol{f} : \mathbb{R}^d \to \mathbb{R}^d$ is the drift vector field and $\boldsymbol{G} \in \mathbb{R}^{d \times m}$ is a constant noise-amplitude matrix. For simplicity, the formulation developed below is presented for additive (or unmodulated) noise. The same framework can be extended to state-dependent (modulated) noise amplitudes.

The stochastic forcing is described by the m-dimensional standard Wiener process

$$\boldsymbol{W}(t) = \begin{bmatrix} W_1(t) & \cdots & W_m(t) \end{bmatrix}^{\mathsf{T}}, \tag{58}$$

where $\mathbb{E}[\boldsymbol{W}(t)] = \boldsymbol{0}$ and $\mathbb{E}\left[\boldsymbol{W}(t)\boldsymbol{W}^{\mathsf{T}}(s)\right] = \min(t,s)\boldsymbol{I}_m$.

The dimension d of the state space and the number m of independent noise sources need not coincide. Writing

$$\boldsymbol{G} = \begin{bmatrix} \boldsymbol{g}_1 & \cdots & \boldsymbol{g}_m \end{bmatrix}, \qquad \boldsymbol{g}_\ell \in \mathbb{R}^d, \tag{59}$$

the vector $\boldsymbol{g}_\ell$ determines how the ℓ^{th} independent noise source acts on the state variables. The matrix $\boldsymbol{G}$ may have rank smaller than either d or m, so the stochastic forcing need not act directly on every component of the state.

The covariance rate of the stochastic increment is

$$\mathbb{E}\left[\left(\boldsymbol{G}\,\mathrm{d}\boldsymbol{W}\right)\left(\boldsymbol{G}\,\mathrm{d}\boldsymbol{W}\right)^{\mathsf{T}}\right] = \boldsymbol{Q}\,\mathrm{d}t, \tag{60}$$

where

$$\boldsymbol{Q} = \boldsymbol{G}\boldsymbol{G}^{\mathsf{T}} \in \mathbb{R}^{d\times d} \tag{61}$$

is positive semidefinite. With the usual Fokker-Planck convention, the corresponding diffusion matrix is

$$\boldsymbol{D} = \frac{1}{2}\boldsymbol{Q} = \frac{1}{2}\boldsymbol{G}\boldsymbol{G}^{\mathsf{T}}. \tag{62}$$

Since $\boldsymbol{G}$ is independent of the state, the stochastic forcing is additive. Consequently, the Itô and Stratonovich interpretations of the stochastic differential equation coincide. The distinction between the two interpretations therefore does not arise in the present formulation.

We assume that the drift vector field is sufficiently regular for the stochastic differential equation to possess a unique solution. The initial condition

$$\boldsymbol{x}(0) = \boldsymbol{x}_0 \tag{63}$$

may be deterministic or random and is assumed to be independent of the future Wiener increments.

The HC method considered here is intended to approximate asymptotically stationary ensemble statistics rather than the transient response associated with a prescribed initial condition. We therefore assume that:

1. The Markov process generated by the stochastic differential equation admits an invariant probability measure $\pi(\mathrm{d}\boldsymbol{x})$.
2. The invariant measure is unique and attracts the probability distribution of the solution for the initial conditions under consideration.
3. The observables and statistical moments considered in the following are integrable with respect to the invariant measure, and the convergence to the invariant measure is sufficiently strong to ensure convergence of their expectations.

Under these assumptions, for any integrable observable $\Phi : \mathbb{R}^d \to \mathbb{R}$, its stationary expectation is

$$\mathbb{E}_{\text{st}}[\Phi] = \int_{\mathbb{R}^d} \Phi(\boldsymbol{x})\,\pi(\mathrm{d}\boldsymbol{x}). \tag{64}$$

Moreover

$$\lim_{t\to+\infty} \mathbb{E}\left[\Phi(\boldsymbol{x}(t))\right] = \mathbb{E}_{\text{st}}[\Phi]. \tag{65}$$

The KL interval $[0,T]$ is kept finite, with T chosen sufficiently large compared with the characteristic relaxation time of the system, so that the distribution of $\boldsymbol{x}(T)$ is sufficiently close to the invariant distribution. Consequently, for the observables of interest,

$$\mathbb{E}\left[\Phi(\boldsymbol{x}(T))\right] \simeq \mathbb{E}_{\text{st}}[\Phi]. \tag{66}$$

3.2 Karhunen-Loève representation of the vector stochastic forcing

Applying the scalar KL representation derived in Section 2.1 to the components of $\boldsymbol{W}(t)$ and retaining the first N modes gives

$$\boldsymbol{W}_N(t) = \sqrt{2T}\sum_{n=1}^{N} \boldsymbol{\zeta}_n \frac{\sin\left[(2n-1)\omega_0 t\right]}{(2n-1)\pi/2}. \tag{67}$$

Each KL mode is associated with an independent Gaussian vector

$$\boldsymbol{\zeta}_n \overset{\text{i.i.d.}}{\sim} \mathcal{N}(\boldsymbol{0}, \boldsymbol{I}_m), \qquad \boldsymbol{\zeta}_n \in \mathbb{R}^m. \tag{68}$$

For fixed N, $\boldsymbol{W}_N(t)$ is a smooth vector-valued Gaussian process. It can therefore be differentiated using the ordinary rules of calculus:

$$\frac{\mathrm{d}\boldsymbol{W}_N(t)}{\mathrm{d}t} = \sqrt{\frac{2}{T}}\sum_{n=1}^{N} \boldsymbol{\zeta}_n \cos\left[(2n-1)\omega_0 t\right]. \tag{69}$$

The covariance and convergence properties established for the scalar approximation in Appendix A hold component-wise.

Collecting all KL coefficients gives the single Gaussian vector

$$\boldsymbol{\zeta} = \begin{bmatrix} \boldsymbol{\zeta}_1^{\mathsf{T}} & \cdots & \boldsymbol{\zeta}_N^{\mathsf{T}} \end{bmatrix}^{\mathsf{T}} \in \mathbb{R}^{mN}, \qquad \boldsymbol{\zeta} \sim \mathcal{N}(\mathbf{0}, \boldsymbol{I}_{mN}). \tag{70}$$

Thus, the stochastic dimension used in the polynomial-chaos representation is $r = mN$.

3.2.1 Correlated Wiener processes

The use of a standard vector Wiener process does not prevent correlated Wiener noise sources from being represented. Let $\widetilde{\boldsymbol{W}}(t) \in \mathbb{R}^m$ be a vector Wiener process with correlated components satisfying

$$\mathbb{E}\left[\widetilde{\boldsymbol{W}}(t)\widetilde{\boldsymbol{W}}^{\mathsf{T}}(s)\right] = \min(t,s)\boldsymbol{R}, \tag{71}$$

where $\boldsymbol{R} \in \mathbb{R}^{m\times m}$ is symmetric and positive semidefinite. Introducing a factorization

$$\boldsymbol{R} = \boldsymbol{L}\boldsymbol{L}^{\mathsf{T}}, \tag{72}$$

the correlated process can be represented as

$$\widetilde{\boldsymbol{W}}(t) = \boldsymbol{L}\boldsymbol{W}(t), \tag{73}$$

where $\boldsymbol{W}(t)$ is a standard vector Wiener process.

Suppose that the correlated process acts on the state through a constant matrix $\boldsymbol{B}$. Then

$$\boldsymbol{B}\,\mathrm{d}\widetilde{\boldsymbol{W}}(t) = \boldsymbol{B}\boldsymbol{L}\,\mathrm{d}\boldsymbol{W}(t). \tag{74}$$

Defining

$$\boldsymbol{G} = \boldsymbol{B}\boldsymbol{L}, \tag{75}$$

the system takes the form introduced in Section 3.1, with independent Wiener processes and noise-amplitude matrix $\boldsymbol{G}$. The covariance rate of the state-space stochastic forcing is

$$\boldsymbol{Q} = \boldsymbol{B}\boldsymbol{R}\boldsymbol{B}^{\mathsf{T}} = \boldsymbol{G}\boldsymbol{G}^{\mathsf{T}}. \tag{76}$$

Thus, correlations between the original noise sources can be included in the deterministic noise-amplitude matrix, while the Gaussian KL coefficients $\boldsymbol{\zeta}_n$ remain independent.

3.3 Vector harmonic-balance formulation

Using the differentiable KL approximation (69), the stochastic differential equation is replaced by

$$\frac{\mathrm{d}\boldsymbol{x}_N(t,\boldsymbol{\zeta})}{\mathrm{d}t} = \boldsymbol{f}\big(\boldsymbol{x}_N(t,\boldsymbol{\zeta})\big) + \sqrt{\frac{2}{T}}\,\boldsymbol{G}\sum_{n=1}^{N}\boldsymbol{\zeta}_n \cos\left[(2n-1)\omega_0 t\right]. \tag{77}$$

For every fixed value of $\boldsymbol{\zeta}$, (77) is an ordinary deterministic differential equation with periodic forcing. All the forcing frequencies are odd multiples of ω_0 and therefore have the common artificial period $\mathcal{T}_0 = 4T$ defined in (21). We apply the harmonic-balance formulation of Section 2.2 and seek a solution having the same period as the forcing. We assume that, for almost every value of $\boldsymbol{\zeta}$, a relevant $\mathcal{T}_0$-periodic solution can be selected consistently and that its harmonic amplitudes are square-integrable functions of $\boldsymbol{\zeta}$.

The selected periodic solution should have an initial state within the basin of attraction of the invariant distribution of the original stochastic system. Under the assumptions introduced in Section 3.1, the stationary statistics are independent of the initial condition within this basin. Their approximation by the HC solution is then subject to the accuracy of the KL, HB, and polynomial-chaos truncations.

The vector harmonic-balance approximation of the state is

$$\boldsymbol{x}_{N,H}(t,\boldsymbol{\zeta}) = \boldsymbol{A}_0(\boldsymbol{\zeta}) + \sum_{k=1}^{H}\left[\boldsymbol{A}_k(\boldsymbol{\zeta})\cos(k\omega_0 t) + \boldsymbol{B}_k(\boldsymbol{\zeta})\sin(k\omega_0 t)\right], \tag{78}$$

where $\boldsymbol{A}_0(\boldsymbol{\zeta})$, $\boldsymbol{A}_k(\boldsymbol{\zeta})$, $\boldsymbol{B}_k(\boldsymbol{\zeta}) \in \mathbb{R}^d$. The harmonic amplitudes are random vectors because they depend on the complete set of Gaussian KL coefficients $\boldsymbol{\zeta} \in \mathbb{R}^{mN}$. In general, each harmonic amplitude depends on all the KL coefficients.

The nonlinear vector field evaluated along (78) is projected onto the retained Fourier basis:

$$\boldsymbol{f}\big(\boldsymbol{x}_{N,H}(t,\boldsymbol{\zeta})\big) \simeq \boldsymbol{F}_0(\boldsymbol{\zeta})$$

$$+\sum_{k=1}^{H}\left[\boldsymbol{F}_k^{(c)}(\boldsymbol{\zeta})\cos(k\omega_0 t)+\boldsymbol{F}_k^{(s)}(\boldsymbol{\zeta})\sin(k\omega_0 t)\right], \tag{79}$$

where

$$\boldsymbol{F}_0(\boldsymbol{\zeta})=\frac{1}{\mathcal{T}_0}\int_0^{\mathcal{T}_0}\boldsymbol{f}\big(\boldsymbol{x}_{N,H}(t,\boldsymbol{\zeta})\big)\,\mathrm{d}t, \tag{80}$$

$$\boldsymbol{F}_k^{(c)}(\boldsymbol{\zeta})=\frac{2}{\mathcal{T}_0}\int_0^{\mathcal{T}_0}\boldsymbol{f}\big(\boldsymbol{x}_{N,H}(t,\boldsymbol{\zeta})\big)\cos(k\omega_0 t)\,\mathrm{d}t, \tag{81}$$

and

$$\boldsymbol{F}_k^{(s)}(\boldsymbol{\zeta})=\frac{2}{\mathcal{T}_0}\int_0^{\mathcal{T}_0}\boldsymbol{f}\big(\boldsymbol{x}_{N,H}(t,\boldsymbol{\zeta})\big)\sin(k\omega_0 t)\,\mathrm{d}t. \tag{82}$$

The additive stochastic forcing contains only the odd cosine harmonics $k=2n-1$ and has no constant or sine components. Equating the coefficients of the same harmonics therefore gives

$$\boldsymbol{F}_0(\boldsymbol{\zeta})=\boldsymbol{0} \tag{83}$$

$$\boldsymbol{F}_k^{(c)}(\boldsymbol{\zeta})+\sqrt{\frac{2}{T}}\,\boldsymbol{G}\sum_{n=1}^{N}\zeta_n\,\delta_{k,\,2n-1} - k\omega_0\boldsymbol{B}_k(\boldsymbol{\zeta})=\boldsymbol{0}, \tag{84}$$

$$\boldsymbol{F}_k^{(s)}(\boldsymbol{\zeta})+k\omega_0\boldsymbol{A}_k(\boldsymbol{\zeta})=\boldsymbol{0}, \tag{85}$$

being $k=1,\dots,H$.

To retain all the forcing modes contained in the N-term KL representation, the harmonic order must satisfy

$$H\geq 2N-1. \tag{86}$$

Higher harmonic orders may be required to represent the harmonics generated by the nonlinear vector field.

For every fixed value of $\boldsymbol{\zeta}$, (83)-(85) form a deterministic nonlinear algebraic system of $d(2H+1)$ scalar equations for the same number of scalar components contained in $\boldsymbol{A}_0(\boldsymbol{\zeta})$, $\boldsymbol{A}_k(\boldsymbol{\zeta})$, and $\boldsymbol{B}_k(\boldsymbol{\zeta})$. As $\boldsymbol{\zeta}$ varies, these harmonic amplitudes define random functions of the KL coefficients. Their polynomial-chaos representations are introduced next.

3.4 Polynomial-chaos representation of the harmonic amplitudes

For every fixed value of $\boldsymbol{\zeta}$, the harmonic-balance equations (83)-(85) determine the harmonic amplitudes $\boldsymbol{A}_0(\boldsymbol{\zeta})$, $\boldsymbol{A}_k(\boldsymbol{\zeta})$, and $\boldsymbol{B}_k(\boldsymbol{\zeta})$. Their dependence on $\boldsymbol{\zeta}$ is therefore defined implicitly by the harmonic-balance system.

We approximate this dependence using the Hermite basis introduced in Section 2.3. The constant harmonic amplitude is written as

$$\boldsymbol{A}_0(\boldsymbol{\zeta})\simeq\sum_{\boldsymbol{\alpha}\in\mathcal{A}_{mN,P}}\boldsymbol{A}_{0,\boldsymbol{\alpha}}\Psi_{\boldsymbol{\alpha}}(\boldsymbol{\zeta}), \tag{87}$$

whereas, for $k=1,\dots,H$,

$$\boldsymbol{A}_k(\boldsymbol{\zeta})\simeq\sum_{\boldsymbol{\alpha}\in\mathcal{A}_{mN,P}}\boldsymbol{A}_{k,\boldsymbol{\alpha}}\Psi_{\boldsymbol{\alpha}}(\boldsymbol{\zeta}), \tag{88}$$

$$\boldsymbol{B}_k(\boldsymbol{\zeta})\simeq\sum_{\boldsymbol{\alpha}\in\mathcal{A}_{mN,P}}\boldsymbol{B}_{k,\boldsymbol{\alpha}}\Psi_{\boldsymbol{\alpha}}(\boldsymbol{\zeta}). \tag{89}$$

Here, $\boldsymbol{A}_{0,\boldsymbol{\alpha}}$, $\boldsymbol{A}_{k,\boldsymbol{\alpha}}$, $\boldsymbol{B}_{k,\boldsymbol{\alpha}}\in\mathbb{R}^d$ are deterministic polynomial-chaos coefficients. For an orthonormal Hermite basis, the exact projection coefficients satisfy

$$\begin{aligned}\boldsymbol{A}_{0,\boldsymbol{\alpha}}&=\mathbb{E}\left[\boldsymbol{A}_0(\boldsymbol{\zeta})\Psi_{\boldsymbol{\alpha}}(\boldsymbol{\zeta})\right],\\ \boldsymbol{A}_{k,\boldsymbol{\alpha}}&=\mathbb{E}\left[\boldsymbol{A}_k(\boldsymbol{\zeta})\Psi_{\boldsymbol{\alpha}}(\boldsymbol{\zeta})\right],\\ \boldsymbol{B}_{k,\boldsymbol{\alpha}}&=\mathbb{E}\left[\boldsymbol{B}_k(\boldsymbol{\zeta})\Psi_{\boldsymbol{\alpha}}(\boldsymbol{\zeta})\right].\end{aligned} \tag{90}$$

These relations characterize the coefficients as orthogonal projections, but their values are not known until the HB system is solved. In the present formulation, they are the deterministic unknowns to be obtained from the coupled Galerkin system presented in Section 3.5.

Substitution into (78) gives the combined temporal-stochastic representation

$$\boldsymbol{x}_{N,H,P}(t,\boldsymbol{\zeta})=\sum_{\boldsymbol{\alpha}\in\mathcal{A}_{mN,P}}\Psi_{\boldsymbol{\alpha}}(\boldsymbol{\zeta})\Bigg\{\boldsymbol{A}_{0,\boldsymbol{\alpha}} +\sum_{k=1}^{H}\left[\boldsymbol{A}_{k,\boldsymbol{\alpha}}\cos(k\omega_0 t)+\boldsymbol{B}_{k,\boldsymbol{\alpha}}\sin(k\omega_0 t)\right]\Bigg\}. \tag{91}$$

Thus, the temporal Fourier representation and the Hermite representation are combined directly

through the deterministic coefficients of the polynomial-chaos expansions of the harmonic amplitudes.

3.5 Coupled temporal-stochastic Galerkin system

The coefficients $\boldsymbol{A}_{0,\boldsymbol{\alpha}}$, $\boldsymbol{A}_{k,\boldsymbol{\alpha}}$, and $\boldsymbol{B}_{k,\boldsymbol{\alpha}}$ are determined by substituting (87)-(89) into the HB system (83)-(85), obtaining a nonlinear system of algebraic equations. Accordingly, in the definitions (80)-(82), the state $\boldsymbol{x}_{N,H}$ is replaced by $\boldsymbol{x}_{N,H,P}$ from (91). The resulting Fourier coefficients of the nonlinear vector field generally depend nonlinearly on the complete set of deterministic polynomial-chaos coefficients.

After this substitution, the HB equations are projected onto the same Hermite basis. For every $\boldsymbol{\beta} \in \mathcal{A}_{mN,P}$, orthonormality gives ($k = 1, \dots, H$)

$$\mathbb{E}\left[\boldsymbol{F}_0(\boldsymbol{\zeta})\Psi_{\boldsymbol{\beta}}(\boldsymbol{\zeta})\right] = \boldsymbol{0}, \tag{92}$$

$$\begin{aligned}\mathbb{E}\left[\boldsymbol{F}_k^{(c)}(\boldsymbol{\zeta})\Psi_{\boldsymbol{\beta}}(\boldsymbol{\zeta})\right] \\ + \sqrt{\frac{2}{T}}\,\boldsymbol{G}\sum_{n=1}^{N}\mathbb{E}\left[\boldsymbol{\zeta}_n\Psi_{\boldsymbol{\beta}}(\boldsymbol{\zeta})\right]\delta_{k,\,2n-1} \\ - k\omega_0\boldsymbol{B}_{k,\boldsymbol{\beta}} = \boldsymbol{0},\end{aligned} \tag{93}$$

$$\mathbb{E}\left[\boldsymbol{F}_k^{(s)}(\boldsymbol{\zeta})\Psi_{\boldsymbol{\beta}}(\boldsymbol{\zeta})\right] + k\omega_0\boldsymbol{A}_{k,\boldsymbol{\beta}} = \boldsymbol{0}. \tag{94}$$

The projection of the stochastic forcing is known explicitly because the components of $\boldsymbol{\zeta}_n$ belong to the first-degree Hermite basis. The expectations involving the Fourier coefficients of the nonlinear vector field couple the temporal harmonics with the stochastic modes and generally depend nonlinearly on all the deterministic coefficients in (87)-(89). Equations (92)-(94) therefore enforce orthogonality of the residual with respect to the retained temporal Fourier modes and stochastic Hermite modes. For polynomial nonlinearities, the stochastic projections can be evaluated algebraically using products of Hermite polynomials. For general nonlinearities, the corresponding expectations can be evaluated by numerical integration.

For every $\boldsymbol{\beta} \in \mathcal{A}_{mN,P}$, the Galerkin system contains $d(2H+1)$ scalar equations. Since

$$|\mathcal{A}_{mN,P}| = \binom{mN+P}{P}, \tag{95}$$

the complete deterministic nonlinear algebraic system contains

$$d(2H+1)\binom{mN+P}{P} \tag{96}$$

scalar equations for the same number of scalar components contained in the vectors $\boldsymbol{A}_{0,\boldsymbol{\alpha}}$, $\boldsymbol{A}_{k,\boldsymbol{\alpha}}$, and $\boldsymbol{B}_{k,\boldsymbol{\alpha}}$. Solving this system determines the polynomial-chaos representation of every harmonic amplitude and hence the combined representation (91).

The coupled nonlinear Galerkin system is solved using a matrix-free Newton–Krylov method, with GMRES employed to solve the linearized systems and a block preconditioner based on the linear harmonic-balance operator. The temporal Fourier projections are evaluated using FFTs, while the stochastic projections are computed algebraically from the Hermite coupling coefficients derived in Appendix B. For the cubic nonlinearity, the polynomial-chaos representation of the squared response is computed once per Newton iteration and reused in the Jacobian-vector products. Continuation from the corresponding linear system is employed to improve convergence.

As in conventional harmonic balance, the coupled HC Galerkin system may admit multiple solutions. Different solutions can be explored by varying the initial guesses for the deterministic HC coefficients in the nonlinear algebraic solver. Each converged solution determines a potentially different HC representation of the stochastic response. The existence of multiple solutions, however, does not by itself establish their dynamical stability or their relevance to the stationary statistics of the original stochastic system.

4 Statistical quantities from the Harmonic Chaos representation

The HC approximation (91) provides a finite-dimensional representation of the stochastic response in terms of the Gaussian vector $\boldsymbol{\zeta}$. Statistical quantities can therefore be expressed as expectations of observables of $\boldsymbol{x}_{N,H,P}(t,\boldsymbol{\zeta})$ with respect to the probability distribution of $\boldsymbol{\zeta}$.

The KL representation of the Wiener process is meaningful only on the interval $[0, T]$, and is extended periodically with period $\mathcal{T}_0 = 4T$ to apply HB. This periodicity is artificial and is not a property of the original stochastic process. Accordingly, only the restriction of the resulting HB solution to $[0, T]$ is interpreted as an approximation of the stochastic response. The periodicity condition implicitly determines the initial state of the selected HB solution. The method is therefore not intended to reproduce the transient associated with an independently prescribed initial condition; the present analysis focuses exclusively on stationary statistical properties. These statistics are estimated by evaluating the response (91) at $t = T$, with T chosen sufficiently large for the distribution of the original stochastic process at that time to be close to its invariant distribution.

For an integrable scalar-, vector-, or matrix-valued observable Φ, the corresponding HC stationary estimate is defined as

$$\mathbb{E}_{\mathrm{HC}}[\Phi] = \mathbb{E}\left[\Phi(\boldsymbol{x}_{N,H,P}(T, \boldsymbol{\zeta}))\right]. \tag{97}$$

In practical computations, T is increased until the statistical quantities of interest become insensitive to further enlargement of the KL interval. For each selected value of T, the truncation orders N, H, and P must also be chosen sufficiently large for the KL, harmonic, and polynomial-chaos truncation errors to be negligible.

At $t = T$,

$$\omega_0 T = \frac{\pi}{2}, \tag{98}$$

so that evaluation of the HC representation (91) at $t = T$ gives

$$\boldsymbol{x}_{N,H,P}(T, \boldsymbol{\zeta}) = \sum_{\boldsymbol{\alpha} \in \mathcal{A}_{mN,P}} \Psi_{\boldsymbol{\alpha}}(\boldsymbol{\zeta}) \Bigg[\boldsymbol{A}_{0,\boldsymbol{\alpha}} + \sum_{k=1}^{\lfloor H/2 \rfloor} (-1)^k \boldsymbol{A}_{2k,\boldsymbol{\alpha}} + \sum_{k=0}^{\lfloor (H-1)/2 \rfloor} (-1)^k \boldsymbol{B}_{2k+1,\boldsymbol{\alpha}} \Bigg], \tag{99}$$

where $\lfloor a \rfloor$ denotes the greatest integer less than or equal to a. The upper summation limits ensure that only harmonics with indices not exceeding H are retained.

The expectation is obtained by projecting the HC representation onto the zero-order Hermite polynomial. Owing to the orthonormality of the Hermite basis, only the zero-order stochastic mode contributes. Therefore,

$$\mathbb{E}_{\mathrm{HC}}[\boldsymbol{x}] = \boldsymbol{A}_{0,\boldsymbol{0}} + \sum_{k=1}^{\lfloor H/2 \rfloor} (-1)^k \boldsymbol{A}_{2k,\boldsymbol{0}} + \sum_{k=0}^{\lfloor (H-1)/2 \rfloor} (-1)^k \boldsymbol{B}_{2k+1,\boldsymbol{0}}. \tag{100}$$

The variance can be obtained directly from the same representation. For a scalar response, subtracting the expectation from (99) removes the zero-order Hermite mode. Squaring the resulting expansion and taking the expectation, the orthonormality of the Hermite polynomials eliminates all cross terms between different stochastic modes. Hence,

$$\mathrm{Var}_{\mathrm{HC}}[x] = \sum_{\substack{\boldsymbol{\alpha} \in \mathcal{A}_{mN,P} \\ \boldsymbol{\alpha} \neq \boldsymbol{0}}} \left[A_{0,\boldsymbol{\alpha}} + \sum_{k=1}^{\lfloor H/2 \rfloor} (-1)^k A_{2k,\boldsymbol{\alpha}} + \sum_{k=0}^{\lfloor (H-1)/2 \rfloor} (-1)^k B_{2k+1,\boldsymbol{\alpha}} \right]^2. \tag{101}$$

For vector-valued responses, the same argument gives the covariance matrix as a sum of outer products of the corresponding nonzero stochastic-mode coefficients. Two-time covariance, autocovariance, and autocorrelation functions can be obtained analogously by evaluating the HC representation at two different times within the KL interval, provided that both times lie in the asymptotically stationary regime.

Higher-order moments of polynomial observables can likewise be evaluated algebraically from the deterministic polynomial-chaos coefficients using the Hermite coupling tensors introduced in Appendix B. In particular, the third- and fourth-order moments can be used to determine skewness and kurtosis without additional stochastic sampling.

4.1 Sampling of the Harmonic Chaos representation

Once the deterministic coefficients $\boldsymbol{A}_{0,\boldsymbol{\alpha}}$, $\boldsymbol{A}_{k,\boldsymbol{\alpha}}$, and $\boldsymbol{B}_{k,\boldsymbol{\alpha}}$ have been computed, different realizations of the stochastic response can be generated without solving the coupled Galerkin

system again. Independent samples $\boldsymbol{\zeta}^{(q)} \sim \mathcal{N}(\mathbf{0}, \boldsymbol{I}_{mN})$, $q = 1, \ldots, N_S$, are generated and substituted directly into (91). Each sample therefore provides a different realization of the HC solution $\boldsymbol{x}_{N,H,P}\left(t, \boldsymbol{\zeta}^{(q)}\right)$, while the deterministic coefficients $\boldsymbol{A}_{0,\boldsymbol{\alpha}}$, $\boldsymbol{A}_{k,\boldsymbol{\alpha}}$, and $\boldsymbol{B}_{k,\boldsymbol{\alpha}}$ remain unchanged.

This provides an inexpensive way to estimate statistical quantities that are not conveniently available in closed form from the polynomial-chaos coefficients. In particular, the stationary probability density function can be estimated from the samples $\boldsymbol{x}_{N,H,P}\left(T, \boldsymbol{\zeta}^{(q)}\right)$, $q = 1, \ldots, N_S$, using standard techniques such as histograms or kernel density estimation [33].

The same samples can also be used to estimate cumulative distribution functions, quantiles, exceedance probabilities, and the probability distributions of nonlinear observables. For example, for a scalar response, the probability of exceeding a prescribed threshold x_c can be estimated as

$$\mathbb{P}\left(x > x_c\right) \simeq \frac{1}{N_S} \sum_{q=1}^{N_S} \mathbb{1}\left[x_{N,H,P}\left(T, \boldsymbol{\zeta}^{(q)}\right) > x_c\right] \tag{102}$$

where $\mathbb{1}[\cdot]$ denotes the indicator function.

Thus, after the initial solution of the coupled temporal-stochastic Galerkin system, Monte Carlo sampling can be performed directly on the HC representation rather than on the original stochastic differential equation.

5 Applications

The HC method is illustrated through two representative examples. The Ornstein-Uhlenbeck process provides a linear benchmark for which the HC representation can be derived analytically and its stationary statistics can be compared with the exact results. The stochastic Duffing oscillator is then considered as a nonlinear example, for which the temporal harmonics and polynomial-chaos modes are coupled by the cubic restoring force. Its known stationary distribution provides a reference for assessing the resulting HC approximation.

5.1 Ornstein-Uhlenbeck Process

Consider the scalar Ornstein-Uhlenbeck process

$$\mathrm{d}x(t) = -\theta\, x(t)\,\mathrm{d}t + \sigma\,\mathrm{d}W(t), \tag{103}$$

where θ and σ are real-valued positive parameters, and $W(t)$ is a standard Wiener process. For the initial condition $x(0) = x_0$, its exact solution is

$$x(t) = x_0 e^{-\theta t} + \sigma \int_0^t e^{-\theta(t-s)}\,\mathrm{d}W(s). \tag{104}$$

The process admits a unique stationary Gaussian distribution

$$p_{\mathrm{st}}(x) = \sqrt{\frac{\theta}{\pi\sigma^2}} \exp\left(-\frac{\theta x^2}{\sigma^2}\right). \tag{105}$$

The corresponding stationary expected value and variance are

$$\mathbb{E}_{\mathrm{st}}[x] = \lim_{t\to\infty} \mathbb{E}[x(t)] = 0,$$
$$\mathrm{Var}_{\mathrm{st}}[x] = \lim_{t\to\infty} \mathbb{E}\left[\left(x(t) - \mathbb{E}[x(t)]\right)^2\right] = \frac{\sigma^2}{2\theta}.$$

Its stationary autocovariance is

$$C_{\mathrm{st}}(\tau) = \lim_{t\to\infty} \mathbb{E}\left[\left(x(t) - \mathbb{E}[x(t)]\right) \times \left(x(t+\tau) - \mathbb{E}[x(t+\tau)]\right)\right] = \frac{\sigma^2}{2\theta} e^{-\theta|\tau|}.$$

5.1.1 Harmonic Chaos solution

Substitution of the N-term KL representation of the white noise into the Ornstein-Uhlenbeck equation gives the random ordinary differential equation

$$\frac{\mathrm{d}x_N(t,\boldsymbol{\zeta})}{\mathrm{d}t} = -\theta x_N(t,\boldsymbol{\zeta}) + \sigma\sqrt{\frac{2}{T}} \sum_{n=1}^{N} \zeta_n \cos\left[(2n-1)\omega_0 t\right], \tag{106}$$

where $\omega_0 = \pi/(2T)$.

For every fixed value of $\boldsymbol{\zeta}$, this is a linear ordinary differential equation with periodic forcing. Since the system is linear, its periodic solution contains only the frequencies present in the KL forcing. The minimum harmonic order required to represent it exactly is therefore $H = 2N - 1$.

The constant harmonic amplitude and all the even harmonic amplitudes vanish ($n = 1, \ldots, N-1$):

$$A_0(\boldsymbol{\zeta}) = 0, \qquad A_{2n}(\boldsymbol{\zeta}) = B_{2n}(\boldsymbol{\zeta}) = 0. \tag{107}$$

For $n = 1, \dots, N$, the nonzero amplitudes are

$$A_{2n-1}(\boldsymbol{\zeta}) = \sigma\sqrt{\frac{2}{T}}\,\frac{\theta}{\theta^2 + [(2n-1)\omega_0]^2}\,\zeta_n, \quad (108)$$

and

$$B_{2n-1}(\boldsymbol{\zeta}) = \sigma\sqrt{\frac{2}{T}}\,\frac{(2n-1)\omega_0}{\theta^2 + [(2n-1)\omega_0]^2}\,\zeta_n. \quad (109)$$

Each harmonic amplitude depends linearly on a single Gaussian KL coefficient. For each $n = 1, \dots, N$, let $\boldsymbol{\alpha} \in \mathbb{N}_0^N$ denote the multi-index such that $\alpha_n = 1$ and $\alpha_j = 0$ for $j \neq n$. Since

$$\Psi_{\boldsymbol{\alpha}}(\boldsymbol{\zeta}) = \zeta_n, \quad (110)$$

the only nonzero deterministic polynomial-chaos coefficients are

$$A_{2n-1,\boldsymbol{\alpha}} = \sigma\sqrt{\frac{2}{T}}\,\frac{\theta}{\theta^2 + [(2n-1)\omega_0]^2}, \quad (111)$$

and

$$B_{2n-1,\boldsymbol{\alpha}} = \sigma\sqrt{\frac{2}{T}}\,\frac{(2n-1)\omega_0}{\theta^2 + [(2n-1)\omega_0]^2}. \quad (112)$$

All the remaining polynomial-chaos coefficients vanish.

The resulting HC representation is therefore

$$x_{N,2N-1,1}(t,\boldsymbol{\zeta}) = \sigma\sqrt{\frac{2}{T}}\sum_{n=1}^{N}\left[\frac{\theta\cos\left[(2n-1)\omega_0 t\right]}{\theta^2 + [(2n-1)\omega_0]^2} + \frac{(2n-1)\omega_0\sin\left[(2n-1)\omega_0 t\right]}{\theta^2 + [(2n-1)\omega_0]^2}\right]\zeta_n. \quad (113)$$

Thus, for the KL-truncated Ornstein-Uhlenbeck equation, harmonic balance is exact for $H \geq 2N-1$, while the first-order polynomial-chaos expansion $P = 1$ is exact because the solution depends linearly on the Gaussian variables. The remaining approximation is due to the finite KL truncation and to the use of a finite interval $[0, T]$.

The left panel of Fig. 2 shows three realizations obtained by evaluating (113) for independent realizations of the Gaussian vector $\boldsymbol{\zeta}$. The KL approximation of the Wiener process was obtained using $N = 10^4$ modes. For the right panel, $N_S = 10^5$ samples $\boldsymbol{\zeta}^{(q)} \sim \mathcal{N}(\mathbf{0}, \boldsymbol{I}_N)$ are generated and the corresponding values $x_{N,2N-1,1}(T, \boldsymbol{\zeta}^{(q)})$ are used to estimate the stationary probability density. The numerical PDF is then compared with the exact stationary Gaussian density (105). Parameter values used in the simulations are $\theta = 1$, $\sigma = 10$.

5.1.2 Expected value, variance, and two-time covariance

Since the HC solution is linear in the centered Gaussian variables ζ_n, its expected value vanishes identically,

$$\mathbb{E}[x_{N,2N-1,1}(t,\boldsymbol{\zeta})] = 0 \quad (114)$$

in agreement with the exact stationary expected value.

At $t = T$,

$$(2n-1)\omega_0 T = \frac{(2n-1)\pi}{2}, \quad (115)$$

so that

$$\cos[(2n-1)\omega_0 T] = 0,$$
$$\sin[(2n-1)\omega_0 T] = (-1)^{n-1}.$$

The HC solution therefore reduces to

$$x_{N,2N-1,1}(T,\boldsymbol{\zeta}) = \sigma\sqrt{\frac{2}{T}}\sum_{n=1}^{N}(-1)^{n-1}\frac{(2n-1)\omega_0}{\theta^2 + [(2n-1)\omega_0]^2}\zeta_n. \quad (116)$$

Since the ζ_n are independent standard Gaussian variables, its variance is

$$\mathrm{Var}_{\mathrm{HC}}[x] = \frac{2\sigma^2}{T}\sum_{n=1}^{N}\frac{[(2n-1)\omega_0]^2}{\{\theta^2 + [(2n-1)\omega_0]^2\}^2}. \quad (117)$$

Using

$$\frac{[(2n-1)\omega_0]^2}{\{\theta^2 + [(2n-1)\omega_0]^2\}^2} = \frac{1}{\theta^2 + [(2n-1)\omega_0]^2} - \frac{\theta^2}{\{\theta^2 + [(2n-1)\omega_0]^2\}^2}, \quad (118)$$

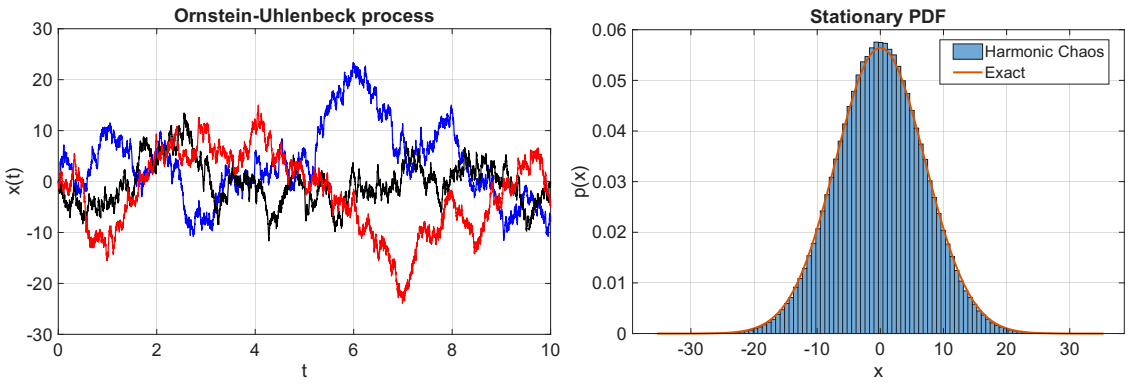


Fig. 2: Left: Three realizations of the Ornstein-Uhlenbeck process obtained from the HC solution (113), corresponding to different realizations of the random vector $\boldsymbol{\zeta}$. Right: Stationary probability density estimated by sampling the HC solution at $t = T$, compared with the exact stationary Gaussian distribution. Parameters used are $\theta = 1$, $\sigma = 10$.

in the infinite-KL-mode limit at fixed finite T, the variance becomes

$$\mathrm{Var}_{\mathrm{HC}}[x] = \frac{2\sigma^2}{T}\left[\sum_{n=1}^{\infty}\frac{1}{\theta^2+[(2n-1)\omega_0]^2} - \theta^2\sum_{n=1}^{\infty}\frac{1}{\{\theta^2+[(2n-1)\omega_0]^2\}^2}\right]. \quad (119)$$

Using the standard summation formula reported in [34, Sec. 1.421.2, p. 44], the first series can be written as

$$\sum_{n=1}^{\infty}\frac{1}{\theta^2+[(2n-1)\omega_0]^2} = \frac{T}{2\theta}\tanh(\theta T). \quad (120)$$

Differentiating this identity with respect to θ yields

$$\sum_{n=1}^{\infty}\frac{1}{\{\theta^2+[(2n-1)\omega_0]^2\}^2} = \frac{T}{4\theta^3}\tanh(\theta T) - \frac{T^2}{4\theta^2}\mathrm{sech}^2(\theta T). \quad (121)$$

Substitution gives

$$\mathrm{Var}_{\mathrm{HC}}[x] = \frac{2\sigma^2}{T}\left[\frac{T}{2\theta}\tanh(\theta T) - \theta^2\left(\frac{T}{4\theta^3}\tanh(\theta T) - \frac{T^2}{4\theta^2}\mathrm{sech}^2(\theta T)\right)\right] = \frac{\sigma^2}{2\theta}\left[\tanh(\theta T) + \theta T\,\mathrm{sech}^2(\theta T)\right]. \quad (122)$$

For a KL interval sufficiently long compared with the relaxation time $1/\theta$,

$$\tanh(\theta T) \simeq 1, \qquad \theta T\,\mathrm{sech}^2(\theta T) \simeq 0, \quad (123)$$

and therefore

$$\mathrm{Var}_{\mathrm{HC}}[x] \simeq \frac{\sigma^2}{2\theta}, \quad (124)$$

recovering the exact stationary variance.

The two-time covariance can be evaluated in the same way. For a fixed lag $0 \le \tau < T$, consider the two states at T and $T-\tau$. Since the mean vanishes, their covariance is

$$C_{\mathrm{HC}}(\tau) = \mathbb{E}\left[x_{N,2N-1,1}(T,\boldsymbol{\zeta})x_{N,2N-1,1}(T-\tau,\boldsymbol{\zeta})\right] = \frac{2\sigma^2}{T}\sum_{n=1}^{N}\left[\frac{\theta(2n-1)\omega_0\sin[(2n-1)\omega_0\tau]}{\{\theta^2+[(2n-1)\omega_0]^2\}^2} + \frac{[(2n-1)\omega_0]^2\cos[(2n-1)\omega_0\tau]}{\{\theta^2+[(2n-1)\omega_0]^2\}^2}\right]. \quad (125)$$

In the infinite-KL-mode limit at fixed finite T, the sums entering the two-time covariance can be evaluated using the standard cosine summation formula reported in [34, Sec. 1.445.2, p. 47]

$$\sum_{k=1}^{\infty}\frac{\cos(kx)}{k^2+a^2} = \frac{\pi}{2a}\frac{\cosh[a(\pi-x)]}{\sinh(\pi a)} - \frac{1}{2a^2}. \quad (126)$$

The sum over the odd harmonics is obtained by subtracting the contribution of the even harmonics from the complete series. The constant terms cancel, giving

$$\sum_{n=1}^{\infty} \frac{\cos[(2n-1)x]}{(2n-1)^2+a^2} = \frac{\pi}{2a}\frac{\cosh[a(\pi-x)]}{\sinh(\pi a)} - \frac{\pi}{4a}\frac{\cosh[a(\pi/2-x)]}{\sinh(\pi a/2)}. \tag{127}$$

Using

$$\sinh(2u) = 2\sinh(u)\cosh(u),$$
$$\cosh(u+v) = \cosh(u)\cosh(v)+\sinh(u)\sinh(v),$$

this expression reduces to

$$\sum_{n=1}^{\infty} \frac{\cos[(2n-1)x]}{(2n-1)^2+a^2} = \frac{\pi}{4a}\frac{\sinh[a(\pi/2-x)]}{\cosh(\pi a/2)}. \tag{128}$$

Finally, setting

$$x = \omega_0\tau, \qquad a = \frac{\theta}{\omega_0}, \qquad \omega_0 = \frac{\pi}{2T}, \tag{129}$$

yields

$$\sum_{n=1}^{\infty} \frac{\cos[(2n-1)\omega_0\tau]}{\theta^2+[(2n-1)\omega_0]^2} = \frac{T}{2\theta}\frac{\sinh[\theta(T-\tau)]}{\cosh(\theta T)}. \tag{130}$$

Differentiation of this identity with respect to θ and τ provides the sums appearing in the two-time covariance, yielding

$$C_{\mathrm{HC}}(\tau) = \frac{\sigma^2}{2\theta}\left[\frac{\sinh[\theta(T-\tau)]}{\cosh(\theta T)} + \theta T e^{\theta\tau}\operatorname{sech}^2(\theta T) - \theta\tau\frac{e^{-\theta(T-\tau)}}{\cosh(\theta T)}\right]. \tag{131}$$

For $\tau = 0$, this expression reduces to the variance obtained above. Moreover, for lags such that $T-\tau$ is sufficiently large compared with the relaxation time $1/\theta$,

$$\frac{\sinh[\theta(T-\tau)]}{\cosh(\theta T)} \simeq e^{-\theta\tau}, \tag{132}$$

whereas the remaining terms are exponentially small. Hence,

$$C_{\mathrm{HC}}(\tau) \simeq \frac{\sigma^2}{2\theta}e^{-\theta\tau}, \quad 0 \le \tau < T,\ T-\tau \gg \frac{1}{\theta} \tag{133}$$

which coincides with the exact stationary autocovariance over the considered range of lags.

Thus, once the KL expansion is sufficiently resolved and the finite interval $[0,T]$ is sufficiently long for both observation times T and $T-\tau$ to lie in the asymptotically stationary regime, the HC representation reproduces the stationary expected value, variance, and autocovariance of the Ornstein-Uhlenbeck process.

5.2 Stochastic Duffing Oscillator

Consider the stochastic Duffing oscillator

$$\ddot{x} + \gamma\dot{x} + k_1 x + k_3 x^3 = \sigma\frac{\mathrm{d}W(t)}{\mathrm{d}t}, \tag{134}$$

where $\gamma > 0$ is the damping coefficient, $k_1 > 0$ is the linear stiffness, $k_3 > 0$ is the cubic stiffness coefficient, and σ denotes the noise amplitude. Introducing the velocity $y = \dot{x}$, the system can equivalently be written as the first-order system of SDEs

$$\mathrm{d}x = y\,\mathrm{d}t, \tag{135}$$

$$\mathrm{d}y = \left(-\gamma y - k_1 x - k_3 x^3\right)\mathrm{d}t + \sigma\,\mathrm{d}W(t). \tag{136}$$

In the following, we restrict the analysis to the monostable case $k_1 > 0$ and $k_3 > 0$. Although the restoring potential has a single minimum, the corresponding periodically forced deterministic system may admit multiple periodic solutions. These solutions can be explored through harmonic balance by varying the initial guesses for the harmonic coefficients. In the present example, we focus on periodic solutions satisfying the symmetry properties discussed below.

The deterministic restoring force derives from the potential

$$U(x) = \frac{k_1}{2}x^2 + \frac{k_3}{4}x^4. \tag{137}$$

The Duffing oscillator possesses a normalizable stationary probability density in the phase space

(x, y),

$$p_{\mathrm{st}}(x, y) = Z^{-1} \exp\left[-\frac{2\gamma}{\sigma^2}\left(\frac{y^2}{2} + U(x)\right)\right], \tag{138}$$

where Z is the partition function.

Integrating with respect to y gives the stationary marginal density of the displacement

$$p_{\mathrm{st}}(x) = Z_x^{-1} \exp\left[-\frac{\gamma}{\sigma^2}\left(k_1\, x^2 + \frac{k_3}{2}\, x^4\right)\right], \tag{139}$$

with

$$Z_x = \int_{-\infty}^{+\infty} \exp\left[-\frac{\gamma}{\sigma^2}\left(k_1\, x^2 + \frac{k_3}{2}\, x^4\right)\right] \mathrm{d}x. \tag{140}$$

Conversely, integrating the stationary density with respect to x gives the stationary marginal density of the velocity,

$$p_{\mathrm{st}}(y) = \sqrt{\frac{\gamma}{\pi\sigma^2}} \exp\left(-\frac{\gamma}{\sigma^2} y^2\right). \tag{141}$$

These analytical stationary distributions provide references for assessing the HC approximation in a genuinely nonlinear system.

Using the differentiated KL approximation of the Wiener process, the stochastic Duffing oscillator becomes

$$\dot{x}_N = y_N \tag{142}$$

$$\dot{y}_N = -\gamma y_N - k_1\, x_N - k_3\, x_N^3 + \sigma\sqrt{\frac{2}{T}} \sum_{n=1}^{N} \zeta_n \cos[(2n-1)\omega_0 t]. \tag{143}$$

The HC formulation introduced in Section 3 can be applied to the stochastic Duffing oscillator. However, the symmetries of the periodically forced system allow the HC representation to be significantly simplified. The forcing in (143) contains only odd harmonics of the fundamental frequency $\omega_0 = \pi/(2T)$. Consequently, it satisfies the half-wave symmetry

$$\eta_N(t + \mathcal{T}_0/2, \boldsymbol{\zeta}) = -\eta_N(t, \boldsymbol{\zeta}), \tag{144}$$

where $\mathcal{T}_0 = 4T$ is the artificial period introduced by the KL representation. Moreover, the restoring force is an odd function of the displacement. We restrict the HC approximation to periodic solutions satisfying the half-wave symmetry

$$x_N(t + \mathcal{T}_0/2, \boldsymbol{\zeta}) = -x_N(t, \boldsymbol{\zeta}). \tag{145}$$

The periodic solution therefore contains only odd temporal harmonics. This symmetry refers exclusively to the periodically extended deterministic system; as discussed in Section 3, only its restriction to $[0, T]$ is used to approximate the stochastic response.

The equation is also invariant under the simultaneous transformations $x \to -x$ and $\boldsymbol{\zeta} \to -\boldsymbol{\zeta}$. We further restrict the HC representation to solutions that preserve the symmetry under simultaneous inversion of the displacement and the Gaussian variables, namely

$$x_N(t, -\boldsymbol{\zeta}) = -x_N(t, \boldsymbol{\zeta}). \tag{146}$$

Consequently, its harmonic amplitudes are odd functions of the Gaussian variables. Since multivariate Hermite polynomials satisfy

$$\Psi_{\boldsymbol{\alpha}}(-\boldsymbol{\zeta}) = (-1)^{|\boldsymbol{\alpha}|} \Psi_{\boldsymbol{\alpha}}(\boldsymbol{\zeta}), \tag{147}$$

only polynomials of odd total degree contribute to their polynomial-chaos expansions.

Combining these two symmetry properties, the HC approximation of the displacement can be written as

$$x_{N,M,P}(t, \boldsymbol{\zeta}) = \sum_{n=1}^{M} \sum_{\boldsymbol{\alpha} \in \mathcal{A}_{N,P}^{\mathrm{odd}}} \Psi_{\boldsymbol{\alpha}}(\boldsymbol{\zeta}) \times \left[A_{n,\boldsymbol{\alpha}} \cos((2n-1)\omega_0 t) + B_{n,\boldsymbol{\alpha}} \sin((2n-1)\omega_0 t)\right], \tag{148}$$

where

$$\mathcal{A}_{N,P}^{\mathrm{odd}} = \{\boldsymbol{\alpha} \in \mathbb{N}_0^N : |\boldsymbol{\alpha}| \le P,\ |\boldsymbol{\alpha}| \text{ odd}\}. \tag{149}$$

Here, $M \ge N$ is the number of retained odd temporal harmonics. The velocity is obtained by differentiating the displacement representation with respect to time.

An important consequence of the stochastic symmetry concerns the polynomial-chaos truncation order. For $P = 2$, only first-degree Hermite polynomials contribute, and the resulting displacement is a linear combination of independent

Table 1: Convergence test of the HC stationary variances with respect to the number L of active KL modes retained in the third-order Hermite expansion. The remaining parameters are fixed at $N = 100$, $M = 110$, and $P = 3$. The quantities ε_x and ε_y denote the relative percentage errors with respect to the corresponding analytical stationary variances.

L	K	$\mathrm{Var}_{HC}(x)$	ε_x (%)	$\mathrm{Var}_{HC}(y)$	ε_y (%)
4	120	0.12349	4.0441	0.14694	5.9584
6	156	0.12395	4.4317	0.14694	5.9584
8	220	0.12262	3.3111	0.14545	6.9120
10	320	0.11388	4.0526	0.15299	2.0864
12	464	0.11322	4.6086	0.15295	2.1120
14	660	0.11325	4.5834	0.15302	2.0672
Exact	–	0.11869	–	0.15625	–

Gaussian variables. Its probability distribution is therefore Gaussian. The lowest polynomial-chaos order capable of representing a non-Gaussian displacement distribution while preserving the symmetry is $P = 3$, which retains Hermite polynomials of total degrees one and three.

The deterministic coefficients of the reduced representation are determined by substituting it into the Duffing equation and imposing Galerkin orthogonality of the residual with respect to the retained temporal and stochastic basis functions. The cubic restoring force preserves both symmetry properties, so that no additional equations arise from projections onto even temporal harmonics or even-degree Hermite polynomials. The nonlinear stochastic projections can be evaluated using the Hermite coupling tensors introduced in Appendix B.

To reduce the computational cost, the numerical implementation employs a sparse Hermite basis obtained by retaining all first-degree polynomials and restricting the third-degree polynomials in $\mathcal{A}^{\mathrm{odd}}_{N,3}$ to $L \leq N$ selected KL variables. The active KL variables are selected according to the amplitudes of the corresponding linear oscillator response.

The resulting number of unknown coefficients is

$$n_{\mathrm{eq}} = 2M \left[N + \binom{L+2}{3} \right]. \tag{150}$$

To improve the robustness of the nonlinear solution, the HC system is solved by continuation in the cubic stiffness coefficient. The procedure starts from the corresponding linear oscillator, obtained by setting $k_3 = 0$, for which the HC coefficients can be computed directly. The coefficient k_3 is then increased gradually from zero to its prescribed value, using the converged HC solution at each continuation step as the initial guess for the following one. In this way, the nonlinear solution is followed continuously from the known linear solution.

The numerical simulations were performed using $\gamma = 0.2$, $k_1 = 1$, $k_3 = 1$, and $\sigma = 0.25$. The KL expansion was defined over the interval $T = 50$ and truncated to $N = 100$ modes. The HC approximation retained $M = 110$ odd temporal harmonics and employed a third-order Hermite expansion ($P = 3$).

A convergence test with respect to L is performed to assess the effect of the sparse Hermite truncation on the stationary statistics. Table 1 reports the stationary variances of displacement and velocity for increasing values of L, while keeping all other numerical parameters fixed. The results are compared with the corresponding analytical stationary variances.

The results indicate convergence of the stationary variances as L increases. Accordingly, $L = 14$ is selected for the subsequent analysis, corresponding to a coupled Galerkin system of 145,200 nonlinear algebraic equations.

Once the deterministic HC coefficients have been computed, different realizations are generated by sampling independent vectors $\boldsymbol{\zeta} \sim \mathcal{N}(\mathbf{0}, \boldsymbol{I}_N)$ and evaluating the HC representation. The samples $x_{N,M,P}(T, \boldsymbol{\zeta})$ can then be used to estimate the stationary displacement distribution and compare it with the analytical stationary density.

Fig. 3 shows three realizations of the stochastic Duffing response obtained for different realizations of the Gaussian vector $\boldsymbol{\zeta}$. The left panel reports

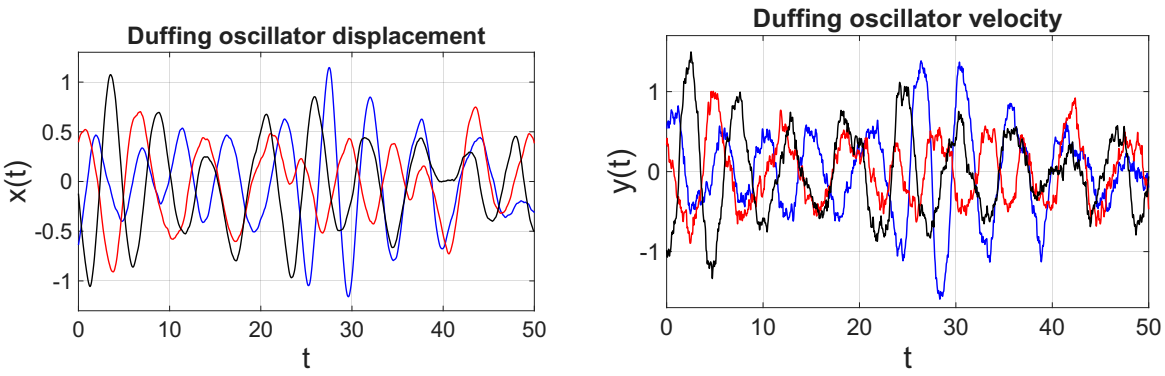


Fig. 3: Left: Three realizations of the displacement $x(t)$ of the stochastic Duffing oscillator obtained from the HC representation for different realizations of the random vector $\boldsymbol{\zeta}$. Right: Corresponding realizations of the velocity $\dot{x}(t) = y(t)$.

the displacement $x(t)$, while the right panel shows the corresponding velocity $y = \dot{x}(t)$. Once a realization of $\boldsymbol{\zeta}$ is specified, the corresponding response is obtained by evaluating the HC representation. The trajectories illustrate the nonlinear stochastic variability of both state variables over the physical interval $0 \leq t \leq T$.

Fig. 4 shows a comparison between the HB solution and that obtained by direct numerical integration of (142), (143), for the same realization of the Gaussian random variables $\boldsymbol{\zeta}$. Initial conditions for the numerical integration were chosen at random, while the initial conditions of the harmonic-balance solution are implicitly determined by the periodicity constraint. The time simulation length is $T = 100$, other parameters are the same reported above. The displacement and velocity obtained with the two methods initially differ because of the different initial conditions but, as expected, after a short transient the two solutions become nearly indistinguishable. The right panel shows the normalized error between the two solutions, defined as $E(t) = \|\widetilde{\boldsymbol{u}}_{\mathrm{ODE}}(t) - \widetilde{\boldsymbol{u}}_{\mathrm{HB}}(t)\|_2$, where $\widetilde{\boldsymbol{u}} = (x/s_x, y/s_y)^{\mathsf{T}}$ is the normalized state vector, and s_x and s_y are the RMS values of the HB displacement and velocity over the second half of the KL interval.

Fig. 5 compares the stationary marginal probability densities obtained from $N_S = 10^5$ numerical samples with the corresponding analytical distributions. The left panel shows the displacement density $p_{\mathrm{st}}(x)$. Owing to the cubic restoring force, the stationary displacement distribution is non-Gaussian and exhibits the characteristic narrowing associated with the quartic contribution to the potential. The right panel shows the stationary velocity density $p_{\mathrm{st}}(y)$. Since the stationary phase-space density is separable in x and y, the velocity marginal is Gaussian, with zero expected value and variance

$$\mathrm{Var}_{\mathrm{st}}[y] = \frac{\sigma^2}{2\gamma}. \tag{151}$$

The Duffing example also illustrates the computational challenges associated with the stochastic dimension of the HC representation. Although the symmetry properties of the system reduce the number of unknowns, the complete third-order Hermite basis still leads to a combinatorial growth of the algebraic system with the number of KL modes. Using a sparse Hermite basis substantially reduces the computational complexity, making possible to retain a relatively large number of KL modes while preserving the nonlinear nature of the response.

Using a reduced basis, sparse Hermite products and a matrix-free Newton-Krylov solver we obtain a computationally tractable implementation of the HC method. However, the selection of the stochastic basis introduces an additional approximation whose accuracy must be assessed through convergence studies with increasing numbers of retained KL variables and polynomial modes.

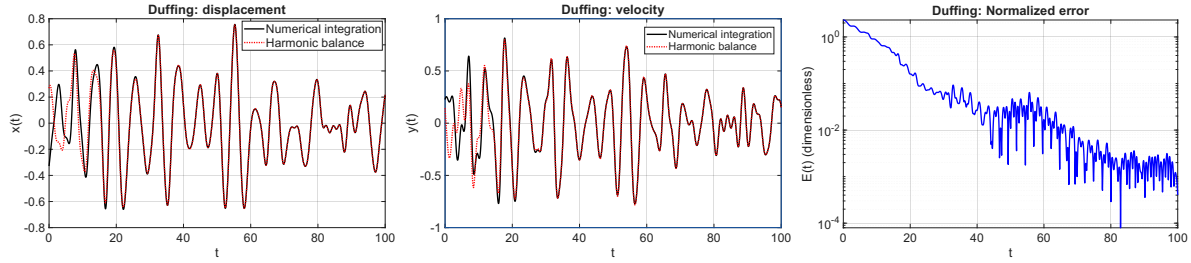


Fig. 4: Comparison between numerical solution (black solid line) and the harmonic balance solution (dotted red line) of (142), (143). Both methods use the same realization of the random forcing. The left and central panels show the displacement and velocity, respectively. The numerical integration starts from randomly generated initial conditions. The right panel shows the normalized error between the two solutions.

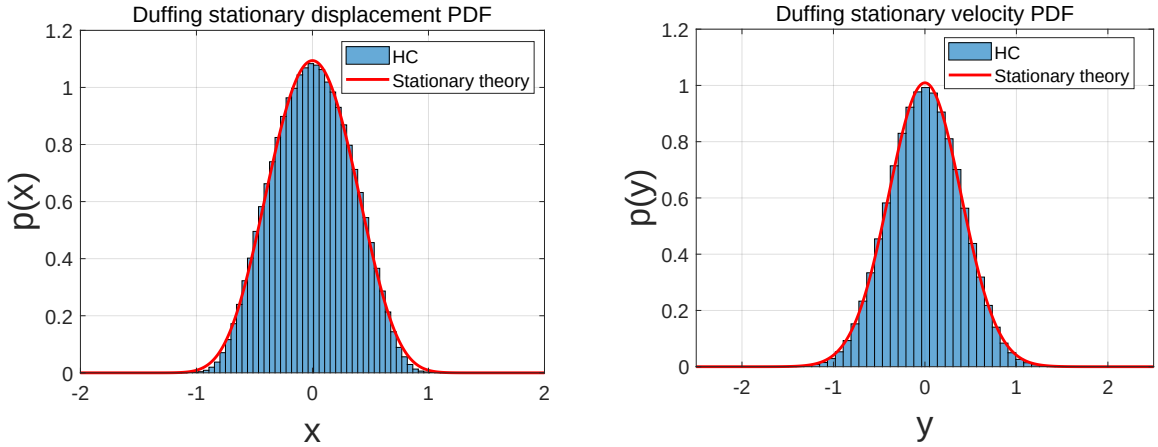


Fig. 5: Left: Stationary probability density of the displacement x, estimated from $N_S = 10^5$ HC samples at $t = T$ and compared with the analytical stationary marginal density. Right: Stationary probability density of the velocity $y = \dot{x}$, compared with the corresponding analytical Gaussian marginal density.

6 Conclusion

Harmonic Chaos provides a mathematical framework for computing stationary statistics of stochastic differential equations driven by Gaussian white noise. By combining a finite-dimensional Karhunen-Loève representation of the Wiener process with harmonic balance and polynomial chaos, the original stochastic differential equation is transformed into a deterministic system of algebraic equations for the temporal-stochastic expansion coefficients. The main computational effort is therefore concentrated in the solution of this algebraic system.

Once the algebraic system is solved, the coefficients permit the direct calculation of expectations, variances, covariance matrices, and correlation functions. At the same time, independent realizations of the stochastic response can be generated at very low additional cost by drawing new realizations of the Gaussian KL variables and evaluating the HC representation, without solving either the original stochastic differential equation or the coupled Galerkin system again. This makes it possible to generate large ensembles efficiently and to estimate quantities such as stationary probability density functions, cumulative distributions, quantiles, and exceedance probabilities.

The Ornstein-Uhlenbeck process is used as a benchmark example. For linear problems, the HC representation can be obtained in closed analytical form. It is shown that the resulting expectation, variance, and autocovariance recover the classical stationary results in the appropriate limits. As an example of application to a genuinely nonlinear problem, we consider the stochastic Duffing oscillator. In nonlinear systems, the temporal harmonics and stochastic modes are coupled by the nonlinear terms. Using a reduced Hermite representation, together with sparse polynomial products and an iterative solution of the coupled Galerkin equations, we obtain a computationally tractable problem. The resulting stationary marginal probability distributions for the displacement and velocity show good agreement with the exact distributions.

The principal limitation of the present formulation is the growth of the number of deterministic coefficients with the number of retained KL variables and the polynomial-chaos order. The Duffing example shows that symmetry and sparse stochastic representations can substantially reduce this cost, but the construction of more systematic adaptive basis-selection strategies remains an important direction for future work. Further developments may also address broader classes of stochastic systems and more efficient numerical implementations of the coupled temporal-stochastic Galerkin problem.

A Properties of the KL approximation of the Wiener process

This appendix collects some statistical properties of the truncated Karhunen-Loève representation of the Wiener process introduced in Section 2.1. In particular, the expectation, variance, and covariance of the finite-dimensional approximation $W_N(t)$ are derived, and the convergence of the differentiated process $\eta_N(t)$ to Gaussian white noise is discussed.

A.1 Expectation, variance, and covariance of the truncated Wiener process

Consider the N-term KL approximation defined in (19),

$$W_N(t) = \sqrt{2T}\sum_{n=1}^{N} \zeta_n \frac{\sin[(2n-1)\omega_0 t]}{(2n-1)\pi/2}, \quad \omega_0 = \frac{\pi}{2T}, \tag{152}$$

where the random variables ζ_n are independent standard Gaussian variables with expectation $\mathbb{E}[\zeta_n] = 0$, and covariance $\mathbb{E}[\zeta_n\zeta_m] = \delta_{nm}$.

The expectation of the truncated process is therefore

$$\mathbb{E}[W_N(t)] = \sqrt{2T}\sum_{n=1}^{N} \frac{\sin[(2n-1)\omega_0 t]}{(2n-1)\pi/2}\mathbb{E}[\zeta_n] = 0. \tag{153}$$

Since the process has zero expectation, its variance is

$$\mathrm{Var}[W_N(t)] = \frac{8T}{\pi^2}\sum_{n=1}^{N} \frac{\sin^2[(2n-1)\omega_0 t]}{(2n-1)^2}. \tag{154}$$

To evaluate the infinite-KL-mode limit, introduce $x = \omega_0 t$, $0 \le x \le \frac{\pi}{2}$. Using $\sin^2 u = [1-\cos(2u)]/2$, and the standard trigonometric-series identity [34, Sec. 1.444.6, p. 47], we obtain, for $0 \le x \le \pi/2$,

$$\sum_{n=1}^{\infty} \frac{\sin^2[(2n-1)x]}{(2n-1)^2} = \frac{\pi x}{4}.$$

Since $x = \omega_0 t$,

$$\sum_{n=1}^{\infty} \frac{\sin^2[(2n-1)\omega_0 t]}{(2n-1)^2} = \frac{\pi\omega_0 t}{4}. \tag{155}$$

Using $\omega_0 = \pi/(2T)$ gives

$$\lim_{N\to\infty} \mathrm{Var}[W_N(t)] = t, \tag{156}$$

recovering the exact variance of the Wiener process.

The covariance of the truncated process is

$$C_{W_N}(t,s) = \mathbb{E}[W_N(t)W_N(s)]. \tag{157}$$

Using $\mathbb{E}[\zeta_n \zeta_m] = \delta_{nm}$ gives

$$C_{W_N}(t,s) = \frac{8T}{\pi^2} \times \sum_{n=1}^{N} \frac{\sin[(2n-1)\omega_0 t]\sin[(2n-1)\omega_0 s]}{(2n-1)^2}. \quad (158)$$

Introduce

$$x = \omega_0 t, \quad y = \omega_0 s, \quad 0 \le x, \quad y \le \frac{\pi}{2}. \quad (159)$$

Using $\sin a \sin b = [\cos(a-b) - \cos(a+b)]/2$, we find

$$\sum_{n=1}^{\infty} \frac{\sin[(2n-1)x]\sin[(2n-1)y]}{(2n-1)^2} = = \frac{1}{2}\sum_{n=1}^{\infty} \frac{\cos[(2n-1)(x-y)]}{(2n-1)^2} - \frac{1}{2}\sum_{n=1}^{\infty} \frac{\cos[(2n-1)(x+y)]}{(2n-1)^2}. \quad (160)$$

Since $|x-y| \le \pi/2$, $0 \le x+y \le \pi$, the same trigonometric-series identity can be applied to both sums, yielding

$$\sum_{n=1}^{\infty} \frac{\sin[(2n-1)x]\sin[(2n-1)y]}{(2n-1)^2} = \frac{\pi}{8}(x+y-|x-y|) = \frac{\pi}{4}\min(x,y). \quad (161)$$

Therefore,

$$\lim_{N\to\infty} C_{W_N}(t,s) = \frac{8T}{\pi^2}\frac{\pi}{4}\min(\omega_0 t, \omega_0 s) = \min(t,s). \quad (162)$$

This is the exact covariance function of the Wiener process.

A.2 Expectation, variance, and covariance of the differentiated KL approximation

For fixed N, $W_N(t)$ is differentiable and its derivative is the smooth Gaussian process defined in (20)

$$\eta_N(t) = \frac{dW_N(t)}{dt} = \sqrt{\frac{2}{T}}\sum_{n=1}^{N} \zeta_n \cos[(2n-1)\omega_0 t]. \quad (163)$$

The process $\eta_N(t)$ is a finite-dimensional approximation of Gaussian white noise, formally defined as the derivative of the Wiener process.

Since $\mathbb{E}[\zeta_n] = 0$, the expectation vanishes for every N,

$$\mathbb{E}[\eta_N(t)] = 0. \quad (164)$$

Using $\mathbb{E}[\zeta_n \zeta_m] = \delta_{nm}$, the variance is

$$\mathrm{Var}[\eta_N(t)] = \frac{2}{T}\sum_{n=1}^{N} \cos^2[(2n-1)\omega_0 t]. \quad (165)$$

Using $\cos^2 u = [1+\cos(2u)]/2$ gives

$$\mathrm{Var}[\eta_N(t)] = \frac{N}{T} + \frac{1}{T}\sum_{n=1}^{N} \cos[2(2n-1)\omega_0 t]. \quad (166)$$

The standard finite trigonometric sum [34, Sec. 1.341.3, p. 36] therefore gives, for $0 < t < T$,

$$\mathrm{Var}[\eta_N(t)] = \frac{N}{T} + \frac{\sin(4N\omega_0 t)}{2T\sin(2\omega_0 t)}. \quad (167)$$

For every fixed $t \in (0,T)$, the second term remains bounded as N increases, whereas the first term grows linearly with N. Hence,

$$\lim_{N\to\infty} \mathrm{Var}[\eta_N(t)] = +\infty. \quad (168)$$

Thus, the differentiated KL approximation reproduces the fact that Gaussian white noise does not possess a finite pointwise variance. At the endpoints, the finite-N approximation satisfies

$$\mathrm{Var}[\eta_N(0)] = \frac{2N}{T}, \qquad \mathrm{Var}[\eta_N(T)] = 0. \quad (169)$$

These special values are boundary effects of the finite-dimensional KL representation.

The covariance of $\eta_N(t)$ is

$$C_{\eta_N}(t,s) = \mathbb{E}[\eta_N(t)\eta_N(s)] = \frac{2}{T}\sum_{n=1}^{N} \cos[(2n-1)\omega_0 t]\cos[(2n-1)\omega_0 s]. \quad (170)$$

For every finite N, this covariance is related to that of the truncated Wiener process by

$$C_{\eta_N}(t,s) = \frac{\partial^2}{\partial t\,\partial s} C_{W_N}(t,s). \tag{171}$$

The infinite series associated with $C_{W_N}(t,s)$ is absolutely and uniformly convergent on $[0,T]^2$. Section A.1 shows that

$$C_{W_N}(t,s) \longrightarrow C_W(t,s) = \min(t,s). \tag{172}$$

Since differentiation is continuous in the space of distributions,

$$C_{\eta_N}(t,s) \longrightarrow \frac{\partial^2}{\partial t\,\partial s} \min(t,s) = \delta(t-s). \tag{173}$$

Here, distributional convergence is understood on $(0,T)\times(0,T)$.

The distributional convergence can also be characterized directly through Parseval's identity. Introduce

$$\phi_n(t) = \sqrt{\frac{2}{T}} \cos[(2n-1)\omega_0 t]. \tag{174}$$

The functions $\{\phi_n\}_{n=1}^{\infty}$ form a complete orthonormal basis of $L^2(0,T)$, and

$$C_{\eta_N}(t,s) = \sum_{n=1}^{N} \phi_n(t)\phi_n(s). \tag{175}$$

For any $h, g \in L^2(0,T)$,

$$\begin{aligned} &\int_0^T \int_0^T h(t) C_{\eta_N}(t,s) g(s)\,\mathrm{d}t\,\mathrm{d}s \\ &\qquad = \sum_{n=1}^{N} \langle h, \phi_n\rangle_{L^2} \langle g, \phi_n\rangle_{L^2}. \end{aligned} \tag{176}$$

Parseval's identity therefore gives

$$\begin{aligned} \lim_{N\to\infty} \int_0^T \int_0^T h(t) C_{\eta_N}(t,s) g(s)\,\mathrm{d}t\,\mathrm{d}s &= \langle h, g\rangle_{L^2} \\ &= \int_0^T h(t) g(t)\,\mathrm{d}t, \end{aligned} \tag{177}$$

which is precisely the action of the white-noise covariance kernel,

$$\int_0^T \int_0^T h(t)\delta(t-s)g(s)\,\mathrm{d}t\,\mathrm{d}s = \int_0^T h(t)g(t)\,\mathrm{d}t. \tag{178}$$

For the vector-valued differentiated KL approximation introduced in Section 3.2, independence of the components of the Gaussian vectors $\boldsymbol{\zeta}_n$ gives

$$\mathbb{E}[\boldsymbol{\eta}_N(t)\boldsymbol{\eta}_N^T(s)] = C_{\eta_N}(t,s)\boldsymbol{I}_m, \tag{179}$$

and therefore

$$\mathbb{E}[\boldsymbol{\eta}(t)\boldsymbol{\eta}^T(s)] = \delta(t-s)\boldsymbol{I}_m. \tag{180}$$

B Additional details on polynomial chaos

This appendix collects algebraic properties of the normalized Hermite basis introduced in Section 2.3 that are useful for evaluating polynomial nonlinearities in the stochastic Galerkin formulation. In particular, explicit product formulas, coupling tensors, and their application to polynomial-chaos projections are presented.

B.1 Normalized Hermite polynomials and multivariate basis functions

The polynomial-chaos basis used in this work is constructed from the normalized probabilists' Hermite polynomials introduced in Section 2.3. The first few univariate polynomials are

$$\psi_0(\zeta) = 1, \tag{181}$$
$$\psi_1(\zeta) = \zeta, \tag{182}$$
$$\psi_2(\zeta) = \frac{\zeta^2 - 1}{\sqrt{2}}, \tag{183}$$
$$\psi_3(\zeta) = \frac{\zeta^3 - 3\zeta}{\sqrt{6}}, \tag{184}$$
$$\psi_4(\zeta) = \frac{\zeta^4 - 6\zeta^2 + 3}{\sqrt{24}}. \tag{185}$$

With respect to the standard Gaussian measure, they satisfy

$$\mathbb{E}[\psi_m(\zeta)\psi_n(\zeta)] = \delta_{mn}. \tag{186}$$

The normalized Hermite polynomials obey the three-term recurrence

$$\zeta\,\psi_p(\zeta) = \sqrt{p+1}\,\psi_{p+1}(\zeta) + \sqrt{p}\,\psi_{p-1}(\zeta),\ p \geq 1, \tag{187}$$

with

$$\zeta\,\psi_0(\zeta) = \psi_1(\zeta). \tag{188}$$

They also satisfy the parity relation

$$\psi_p(-\zeta) = (-1)^p \psi_p(\zeta). \tag{189}$$

These properties are useful in determining which polynomial modes are coupled by products of Hermite polynomials.

For a vector of independent standard Gaussian variables

$$\boldsymbol{\zeta} = [\zeta_1, \ldots, \zeta_r]^T, \qquad \zeta_j \overset{\text{i.i.d.}}{\sim} \mathcal{N}(0,1), \tag{190}$$

the multivariate Hermite polynomial associated with the multi-index

$$\boldsymbol{\alpha} = (\alpha_1, \ldots, \alpha_r) \tag{191}$$

is obtained as the tensor product

$$\Psi_{\boldsymbol{\alpha}}(\boldsymbol{\zeta}) = \prod_{j=1}^{r} \psi_{\alpha_j}(\zeta_j). \tag{192}$$

Its total polynomial degree is

$$|\boldsymbol{\alpha}| = \sum_{j=1}^{r} \alpha_j. \tag{193}$$

For example, for $r = 3$ and

$$\boldsymbol{\alpha} = (3, 2, 4), \tag{194}$$

the corresponding multivariate basis function is

$$\begin{aligned}\Psi_{(3,2,4)}(\boldsymbol{\zeta}) &= \psi_3(\zeta_1)\psi_2(\zeta_2)\psi_4(\zeta_3) \\ &= \frac{\zeta_1^3 - 3\zeta_1}{\sqrt{6}} \frac{\zeta_2^2 - 1}{\sqrt{2}} \frac{\zeta_3^4 - 6\zeta_3^2 + 3}{\sqrt{24}},\end{aligned} \tag{195}$$

with total degree

$$|\boldsymbol{\alpha}| = 3 + 2 + 4 = 9. \tag{196}$$

B.2 Products of normalized Hermite polynomials

The product of two normalized univariate Hermite polynomials can be expanded in the same basis according to the linearization formula

$$\begin{aligned}\psi_m(\zeta)\psi_n(\zeta) = &\sum_{\ell=0}^{\min(m,n)} \ell! \binom{m}{\ell} \binom{n}{\ell} \\ &\times \sqrt{\frac{(m+n-2\ell)!}{m!\,n!}}\,\psi_{m+n-2\ell}(\zeta).\end{aligned} \tag{197}$$

Thus, only polynomial degrees

$$m+n,\ m+n-2,\ \ldots,\ |m-n| \tag{198}$$

appear in the product. In particular, all resulting degrees have the same parity as $m+n$.

The univariate triple-product coefficient is defined as

$$c_{mnp} = \mathbb{E}[\psi_m(\zeta)\psi_n(\zeta)\psi_p(\zeta)]. \tag{199}$$

By orthonormality, c_{mnp} is precisely the coefficient of $\psi_p(\zeta)$ in the linearization formula above. Introducing

$$\begin{aligned}a &= \frac{m+n-p}{2}, \\ b &= \frac{m+p-n}{2}, \\ c &= \frac{n+p-m}{2},\end{aligned}$$

the coefficient can be written explicitly as

$$c_{mnp} = \begin{cases} \dfrac{\sqrt{m!\,n!\,p!}}{a!\,b!\,c!}, & a,b,c \in \mathbb{N}_0, \\ 0, & \text{otherwise.} \end{cases} \tag{200}$$

The coefficient c_{mnp} is invariant under any permutation of the indices m, n, and p.

Consequently, c_{mnp} is nonzero if and only if $m+n+p$ is even and the three polynomial degrees satisfy the triangle inequalities

$$m+n \geq p, \qquad m+p \geq n, \qquad n+p \geq m. \tag{201}$$

For example,

$$\psi_1^2(\zeta) = \psi_0(\zeta) + \sqrt{2}\,\psi_2(\zeta), \tag{202}$$

so that

$$c_{110} = 1, \qquad c_{112} = \sqrt{2}, \tag{203}$$

whereas $c_{11p} = 0$ for all other values of p. This simple example illustrates both the parity and degree selection rules.

For a total-degree truncation with $P = 3$, as used in the Duffing example of Section 5.2, these componentwise selection rules eliminate the large majority of formally possible multivariate couplings. They are therefore responsible for the sparsity of the coupling tensors introduced below.

B.3 Multivariate coupling tensors

For the multivariate Hermite basis, define the third-order coupling tensor

$$C_{\boldsymbol{\alpha}\boldsymbol{\beta}\boldsymbol{\gamma}} = \mathbb{E}[\Psi_{\boldsymbol{\alpha}}(\boldsymbol{\zeta})\Psi_{\boldsymbol{\beta}}(\boldsymbol{\zeta})\Psi_{\boldsymbol{\gamma}}(\boldsymbol{\zeta})]. \tag{204}$$

Since

$$\Psi_{\boldsymbol{\alpha}}(\boldsymbol{\zeta})\Psi_{\boldsymbol{\beta}}(\boldsymbol{\zeta})\Psi_{\boldsymbol{\gamma}}(\boldsymbol{\zeta}) = \prod_{j=1}^{r} \psi_{\alpha_j}(\zeta_j)\psi_{\beta_j}(\zeta_j)\psi_{\gamma_j}(\zeta_j), \tag{205}$$

independence of the Gaussian variables gives

$$C_{\boldsymbol{\alpha}\boldsymbol{\beta}\boldsymbol{\gamma}} = \prod_{j=1}^{r} c_{\alpha_j\beta_j\gamma_j}, \tag{206}$$

where the univariate triple-product coefficients c_{mnp} are given in Section B.2.

The tensor $C_{\boldsymbol{\alpha}\boldsymbol{\beta}\boldsymbol{\gamma}}$ is invariant under permutations of its three multi-indices. Moreover, it is sparse because it can be nonzero only if the univariate selection rules of Section B.2 are satisfied for every component $j = 1, \dots, r$.

Similarly, define the fourth-order coupling tensor

$$D_{\boldsymbol{\alpha}\boldsymbol{\beta}\boldsymbol{\gamma}\boldsymbol{\delta}} = \mathbb{E}[\Psi_{\boldsymbol{\alpha}}(\boldsymbol{\zeta})\Psi_{\boldsymbol{\beta}}(\boldsymbol{\zeta})\Psi_{\boldsymbol{\gamma}}(\boldsymbol{\zeta})\Psi_{\boldsymbol{\delta}}(\boldsymbol{\zeta})]. \tag{207}$$

Introducing the univariate fourth-order coefficient

$$d_{mnpq} = \mathbb{E}[\psi_m(\zeta)\psi_n(\zeta)\psi_p(\zeta)\psi_q(\zeta)], \tag{208}$$

independence gives

$$D_{\boldsymbol{\alpha}\boldsymbol{\beta}\boldsymbol{\gamma}\boldsymbol{\delta}} = \prod_{j=1}^{r} d_{\alpha_j\beta_j\gamma_j\delta_j}. \tag{209}$$

The univariate fourth-order coefficient can be expressed in terms of the triple-product coefficients. Expanding the products $\psi_m\psi_n$ and $\psi_p\psi_q$ in the Hermite basis and using orthonormality gives

$$d_{mnpq} = \sum_{k=0}^{\infty} c_{mnk}\, c_{pqk}. \tag{210}$$

Only finitely many terms in this sum are nonzero. Consequently,

$$D_{\boldsymbol{\alpha}\boldsymbol{\beta}\boldsymbol{\gamma}\boldsymbol{\delta}} = \sum_{\boldsymbol{\kappa}\in\mathbb{N}_0^r} C_{\boldsymbol{\alpha}\boldsymbol{\beta}\boldsymbol{\kappa}} C_{\boldsymbol{\gamma}\boldsymbol{\delta}\boldsymbol{\kappa}}. \tag{211}$$

A term in this sum can be nonzero only if

$$|\boldsymbol{\kappa}| \le \min(|\boldsymbol{\alpha}| + |\boldsymbol{\beta}|, |\boldsymbol{\gamma}| + |\boldsymbol{\delta}|)\,. \tag{212}$$

Hence, if $\boldsymbol{\alpha}, \boldsymbol{\beta}, \boldsymbol{\gamma}, \boldsymbol{\delta} \in \mathcal{A}_{r,P}$, then necessarily $|\boldsymbol{\kappa}| \le 2P$, and the fourth-order tensor can be written as

$$D_{\boldsymbol{\alpha}\boldsymbol{\beta}\boldsymbol{\gamma}\boldsymbol{\delta}} = \sum_{\boldsymbol{\kappa}\in\mathcal{A}_{r,2P}} C_{\boldsymbol{\alpha}\boldsymbol{\beta}\boldsymbol{\kappa}} C_{\boldsymbol{\gamma}\boldsymbol{\delta}\boldsymbol{\kappa}}, \tag{213}$$

with the understanding that the selection rules eliminate most of the terms in the sum. The intermediate multi-index $\boldsymbol{\kappa}$ must therefore not, in general, be restricted to the original truncation set $\mathcal{A}_{r,P}$.

The tensor $D_{\boldsymbol{\alpha}\boldsymbol{\beta}\boldsymbol{\gamma}\boldsymbol{\delta}}$ is invariant under any permutation of its four multi-indices. More generally, let

$$\boldsymbol{\alpha}_q = (\alpha_{q,1}, \dots, \alpha_{q,r}), \qquad q = 1, \dots, s. \tag{214}$$

The coupling tensor associated with the product of s multivariate basis functions is

$$H_{\boldsymbol{\alpha}_1\cdots\boldsymbol{\alpha}_s} = \mathbb{E}\left[\prod_{q=1}^{s} \Psi_{\boldsymbol{\alpha}_q}(\boldsymbol{\zeta})\right]. \tag{215}$$

Independence of the Gaussian variables yields

$$H_{\boldsymbol{\alpha}_1\cdots\boldsymbol{\alpha}_s} = \prod_{j=1}^{r} \mathbb{E}\left[\prod_{q=1}^{s} \psi_{\alpha_{q,j}}(\zeta_j)\right]. \tag{216}$$

Thus, multivariate coupling tensors can be constructed entirely from the corresponding univariate Gaussian expectations. Their sparsity and

symmetry can be exploited when evaluating nonlinear polynomial-chaos projections.

B.4 Polynomial-chaos projection of nonlinear products

Consider scalar polynomial-chaos expansions, or scalar components of vector-valued expansions, truncated on the total-degree index set $\mathcal{A}_{r,P}$. For a square-integrable scalar function $F(\boldsymbol{\zeta})$, its orthogonal projection onto the retained polynomial space is

$$\Pi_P[F] = \sum_{\boldsymbol{\gamma}\in\mathcal{A}_{r,P}} \mathbb{E}[F(\boldsymbol{\zeta})\Psi_{\boldsymbol{\gamma}}(\boldsymbol{\zeta})]\Psi_{\boldsymbol{\gamma}}(\boldsymbol{\zeta}). \tag{217}$$

Consider two truncated expansions

$$Y_P(\boldsymbol{\zeta}) = \sum_{\boldsymbol{\alpha}\in\mathcal{A}_{r,P}} y_{\boldsymbol{\alpha}}\Psi_{\boldsymbol{\alpha}}(\boldsymbol{\zeta}), \tag{218}$$

and

$$Z_P(\boldsymbol{\zeta}) = \sum_{\boldsymbol{\beta}\in\mathcal{A}_{r,P}} z_{\boldsymbol{\beta}}\Psi_{\boldsymbol{\beta}}(\boldsymbol{\zeta}). \tag{219}$$

Their product generally contains polynomial modes of total degree up to $2P$ and therefore does not, in general, belong to the original truncated space. Its projection onto $\mathcal{A}_{r,P}$ can be written as

$$\Pi_P[Y_P Z_P] = \sum_{\boldsymbol{\gamma}\in\mathcal{A}_{r,P}} q^{(2)}_{\boldsymbol{\gamma}}\Psi_{\boldsymbol{\gamma}}(\boldsymbol{\zeta}), \tag{220}$$

where

$$\begin{aligned} q^{(2)}_{\boldsymbol{\gamma}} &= \mathbb{E}[Y_P(\boldsymbol{\zeta})Z_P(\boldsymbol{\zeta})\Psi_{\boldsymbol{\gamma}}(\boldsymbol{\zeta})] \\ &= \sum_{\boldsymbol{\alpha}\in\mathcal{A}_{r,P}}\sum_{\boldsymbol{\beta}\in\mathcal{A}_{r,P}} y_{\boldsymbol{\alpha}} z_{\boldsymbol{\beta}} C_{\boldsymbol{\alpha}\boldsymbol{\beta}\boldsymbol{\gamma}}. \end{aligned} \tag{221}$$

Thus, the third-order coupling tensor provides directly the Galerkin coefficients of a quadratic product.

Similarly, the third power of an expansion contains polynomial modes of total degree up to $3P$. Its projection onto the retained space is

$$\Pi_P[Y_P^3] = \sum_{\boldsymbol{\delta}\in\mathcal{A}_{r,P}} q^{(3)}_{\boldsymbol{\delta}}\Psi_{\boldsymbol{\delta}}(\boldsymbol{\zeta}), \tag{222}$$

with

$$\begin{aligned} q^{(3)}_{\boldsymbol{\delta}} &= \mathbb{E}[Y_P^3(\boldsymbol{\zeta})\Psi_{\boldsymbol{\delta}}(\boldsymbol{\zeta})] \\ &= \sum_{\boldsymbol{\alpha}\in\mathcal{A}_{r,P}}\sum_{\boldsymbol{\beta}\in\mathcal{A}_{r,P}}\sum_{\boldsymbol{\kappa}\in\mathcal{A}_{r,P}} y_{\boldsymbol{\alpha}} y_{\boldsymbol{\beta}} y_{\boldsymbol{\kappa}} D_{\boldsymbol{\alpha}\boldsymbol{\beta}\boldsymbol{\kappa}\boldsymbol{\delta}}. \end{aligned} \tag{223}$$

The fourth-order tensor therefore gives the stochastic Galerkin projection of cubic nonlinearities, such as the restoring force in the Duffing oscillator of Section 5.2.

In practice, the cubic projection need not be evaluated through the dense triple contraction above. Using the decomposition of the fourth-order tensor in terms of third-order coupling coefficients, the quadratic intermediate coefficients are first computed as

$$u_{\boldsymbol{\kappa}} = \sum_{\boldsymbol{\alpha}\in\mathcal{A}_{r,P}}\sum_{\boldsymbol{\beta}\in\mathcal{A}_{r,P}} y_{\boldsymbol{\alpha}} y_{\boldsymbol{\beta}} C_{\boldsymbol{\alpha}\boldsymbol{\beta}\boldsymbol{\kappa}}, \quad \boldsymbol{\kappa}\in\mathcal{A}_{r,2P}. \tag{224}$$

The cubic projection coefficients are then obtained from

$$q^{(3)}_{\boldsymbol{\delta}} = \sum_{\boldsymbol{\kappa}\in\mathcal{A}_{r,2P}}\sum_{\boldsymbol{\lambda}\in\mathcal{A}_{r,P}} u_{\boldsymbol{\kappa}} y_{\boldsymbol{\lambda}} C_{\boldsymbol{\kappa}\boldsymbol{\lambda}\boldsymbol{\delta}}, \quad \boldsymbol{\delta}\in\mathcal{A}_{r,P}. \tag{225}$$

The intermediate quadratic expansion must be retained up to total degree $2P$: projecting it prematurely onto $\mathcal{A}_{r,P}$ may discard modes that contribute to the final projection of the cubic term. The two-step formulation avoids forming the fourth-order tensor explicitly and allows the sparsity of $C_{\boldsymbol{\alpha}\boldsymbol{\beta}\boldsymbol{\gamma}}$ to be exploited in both contractions.

More generally, let

$$Y^{(j)}_P(\boldsymbol{\zeta}) = \sum_{\boldsymbol{\alpha}_j\in\mathcal{A}_{r,P}} y^{(j)}_{\boldsymbol{\alpha}_j}\Psi_{\boldsymbol{\alpha}_j}(\boldsymbol{\zeta}), \qquad j = 1,\dots,s. \tag{226}$$

The projection of their product is

$$\Pi_P\left[\prod_{j=1}^{s} Y^{(j)}_P\right] = \sum_{\boldsymbol{\gamma}\in\mathcal{A}_{r,P}} q^{(s)}_{\boldsymbol{\gamma}}\Psi_{\boldsymbol{\gamma}}(\boldsymbol{\zeta}), \tag{227}$$

where

$$\begin{aligned} q^{(s)}_{\boldsymbol{\gamma}} &= \mathbb{E}\left[\left(\prod_{j=1}^{s} Y^{(j)}_P\right)\Psi_{\boldsymbol{\gamma}}(\boldsymbol{\zeta})\right] \\ &= \sum_{\boldsymbol{\alpha}_1,\dots,\boldsymbol{\alpha}_s\in\mathcal{A}_{r,P}} \left(\prod_{j=1}^{s} y^{(j)}_{\boldsymbol{\alpha}_j}\right) H_{\boldsymbol{\alpha}_1\cdots\boldsymbol{\alpha}_s\boldsymbol{\gamma}}. \end{aligned} \tag{228}$$

Hence, polynomial nonlinearities of arbitrary degree can be projected onto the retained polynomial-chaos space through contractions with the coupling tensors defined in Section B.3.

The coupling tensors describe the stochastic part of the nonlinear projection. In the HC formulation, this contraction is combined with the convolution of the temporal Fourier coefficients. For compactness, consider the equivalent complex Fourier representation of a scalar component,

$$x_{H,P}(t,\boldsymbol{\zeta}) = \sum_{k=-H}^{H} \sum_{\boldsymbol{\alpha}\in\mathcal{A}_{r,P}} \widehat{x}_{k,\boldsymbol{\alpha}} e^{ik\omega_0 t} \Psi_{\boldsymbol{\alpha}}(\boldsymbol{\zeta}). \tag{229}$$

The coefficient of the projected cubic term associated with temporal harmonic k and stochastic mode $\boldsymbol{\delta}$ is

$$\widehat{(x^3)}_{k,\boldsymbol{\delta}} = \sum_{\substack{k_1+k_2+k_3=k \\ |k_1|,|k_2|,|k_3|\le H}} \tag{230}$$

$$\times \sum_{\boldsymbol{\alpha},\boldsymbol{\beta},\boldsymbol{\kappa}\in\mathcal{A}_{r,P}} \widehat{x}_{k_1,\boldsymbol{\alpha}} \widehat{x}_{k_2,\boldsymbol{\beta}} \widehat{x}_{k_3,\boldsymbol{\kappa}} D_{\boldsymbol{\alpha}\boldsymbol{\beta}\boldsymbol{\kappa}\boldsymbol{\delta}}, \tag{231}$$

for $|k| \le H$ and $\boldsymbol{\delta} \in \mathcal{A}_{r,P}$. Thus, polynomial nonlinearities generate simultaneously a convolution over temporal harmonics and a contraction over stochastic modes. The real sine-cosine formulation used in the main text is equivalent to this complex representation.

The required coupling coefficients depend only on the Hermite basis and on the retained index sets and can therefore be precomputed and reused throughout the solution of the stochastic Galerkin system. Their sparsity, inherited from the univariate selection rules, substantially reduces the number of nonzero contractions required in practical computations.

Declarations

Funding. No funding information is currently provided.

Competing interests. The authors declare no competing interests.

Data availability. The data and code used to generate the numerical results will be made available upon reasonable request, or a repository link will be added before submission.

Author contributions. All authors contributed equally to the manuscript.

References

[1] Demir, A., Mehrotra, A., Roychowdhury, J.: Phase noise in oscillators: a unifying theory and numerical methods for characterization. IEEE Transactions on Circuits and Systems I: Fundamental Theory and Applications **47**(5), 655–674 (2000) https://doi.org/10.1109/81.847872

[2] Bonnin, M., Corinto, F.: Phase noise and noise induced frequency shift in stochastic nonlinear oscillators. IEEE Transactions on Circuits and Systems I: Regular Papers **60**(8), 2104–2115 (2013) https://doi.org/10.1109/TCSI.2013.2239131

[3] Bonnin, M., Traversa, F.L., Bonani, F.: Colored noise in oscillators. phase-amplitude analysis and a method to avoid the Itô-Stratonovich dilemma. IEEE Transactions on Circuits and Systems I: Regular Papers **66**(10), 3917–3927 (2019) https://doi.org/10.1109/TCSI.2019.2914398

[4] Bonnin, M., Van Brandt, L., Delvenne, J.-C., Traversa, F.L., Bonani, F.: A thermodynamically consistent thermal equilibrium Gaussian white noise model for nonlinear resistors. IEEE Transactions on Circuits and Systems I: Regular Papers **73**(6), 3901–3913 (2026) https://doi.org/10.1109/TCSI.2025.3639450

[5] Lin, Y.K., Kozin, F., Wen, Y.K., Casciati, F., Schuëller, G.I., Der Kiureghian, A., Ditlevsen, O., Vanmarcke, E.H.: Methods of stochastic structural dynamics. Structural Safety **3**(3), 167–194 (1986) https://doi.org/10.1016/0167-4730(86)90003-2

[6] Zhu, W.Q.: Theory of stochastically excited and dissipated hamiltonian systems — some new developments in nonlinear stochastic structural dynamics. Advances in Structural Engineering **2**(3), 173–189 (1999) https://doi.org/10.1177/136943329900200302

[7] Bonnin, M., Song, K., Traversa, F.L., Bonani, F.: Model order reduction and stochastic

averaging for the analysis and design of micro-electro-mechanical systems. Nonlinear Dynamics **112**(5), 3421–3439 (2024)

[8] Song, K., Bonnin, M., Traversa, F.L., Bonani, F.: Broadband vibration energy harvesting using nonlinear multi degree-of-freedom mechanical filters. Nonlinear Dynamics **113**(12), 14301–14317 (2025)

[9] Gammaitoni, L., Hänggi, P., Jung, P., Marchesoni, F.: Stochastic resonance. Rev. Mod. Phys. **70**, 223–287 (1998) https://doi.org/10.1103/RevModPhys.70.223

[10] Hänggi, P., Marchesoni, F.: Artificial brownian motors: Controlling transport on the nanoscale. Rev. Mod. Phys. **81**, 387–442 (2009) https://doi.org/10.1103/RevModPhys.81.387

[11] Seifert, U.: Stochastic thermodynamics, fluctuation theorems and molecular machines. Reports on progress in physics **75**(12), 126001 (2012)

[12] Giles, M.B.: Multilevel monte carlo path simulation. Operations research **56**(3), 607–617 (2008)

[13] Giles, M.B.: Multilevel monte carlo methods. Acta Numerica **24**, 259–328 (2015) https://doi.org/10.1017/S096249291500001X

[14] Spencer Jr, B., Bergman, L.: On the numerical solution of the fokker-planck equation for nonlinear stochastic systems. Nonlinear Dynamics **4**(4), 357–372 (1993)

[15] Wang, X., Jiang, J., Hong, L., Sun, J.-Q.: A novel method for response probability density of nonlinear stochastic dynamic systems. Nonlinear Dynamics **113**(5), 3981–3997 (2025)

[16] Bobryk, R.V.: Closure schemes in stochastic nonlinear dynamics: A validation case study. Phys. Rev. E **83**, 057701 (2011) https://doi.org/10.1103/PhysRevE.83.057701

[17] Potenza, F., Gattulli, V., Vasta, M.: Optimization of a viscous-elastic damper coupling two simple oscillators based on nonlinear stochastic response. Nonlinear Dynamics **113**(22), 30427–30442 (2025)

[18] Ghanem, R.G., Spanos, P.D.: Spectral stochastic finite-element formulation for reliability analysis. Journal of Engineering Mechanics **117**(10), 2351–2372 (1991)

[19] Xiu, D., Karniadakis, G.E.: The Wiener–Askey polynomial chaos for stochastic differential equations. SIAM Journal on Scientific Computing **24**(2), 619–644 (2002) https://doi.org/10.1137/S1064827501387826

[20] Gerritsma, M., van der Steen, J.-B., Vos, P., Karniadakis, G.: Time-dependent generalized polynomial chaos. Journal of Computational Physics **229**(22), 8333–8363 (2010) https://doi.org/10.1016/j.jcp.2010.07.020

[21] Ozen, H.C., Bal, G.: Dynamical polynomial chaos expansions and long time evolution of differential equations with random forcing. SIAM/ASA Journal on Uncertainty Quantification **4**(1), 609–635 (2016) https://doi.org/10.1137/15M1019167

[22] Cameron, T.M., Griffin, J.H.: An alternating frequency/time domain method for calculating the steady-state response of nonlinear dynamic systems. Journal of Applied Mechanics **56**(1), 149–154 (1989) https://doi.org/10.1115/1.3176036

[23] Bonani, F., Gilli, M.: Analysis of stability and bifurcations of limit cycles in chua's circuit through the harmonic-balance approach. IEEE Transactions on Circuits and Systems I: Fundamental Theory and Applications **46**(8), 881–890 (1999) https://doi.org/10.1109/81.780370

[24] Detroux, T., Renson, L., Masset, L., Kerschen, G.: The harmonic balance method for bifurcation analysis of large-scale nonlinear mechanical systems. Computer Methods in Applied Mechanics and Engineering **296**, 18–38 (2015)

[25] Hayes, R., Marques, S.P.: Prediction of limit cycle oscillations under uncertainty using a harmonic balance method. Computers & Structures **148**, 1–13 (2015) https://doi.org/10.1016/j.compstruc.2014.10.010

[26] Trinh, M.-H., Berger, S., Aubry, E.: Nonlinear dynamic behaviour analysis of a clutch system with uncertainties using polynomial chaos and the constrained harmonic balance method. Shock and Vibration **2020**, 1–14 (2020) https://doi.org/10.1155/2020/8401745

[27] Karhunen, K.: Über lineare methoden in der wahrscheinlichkeitsrechnung. Annales Academiae Scientiarum Fennicae. Series A I. Mathematica-Physica **37**, 1–79 (1947)

[28] Loève, M.: Probability Theory I, 4th edn. Graduate Texts in Mathematics, vol. 45. Springer, New York (1977). https://doi.org/10.1007/978-1-4684-9464-8

[29] Ghanem, R.G., Spanos, P.D.: Stochastic Finite Elements: A Spectral Approach. Springer, New York (1991). https://doi.org/10.1007/978-1-4612-3094-6

[30] Urabe, M.: Galerkin's procedure for nonlinear periodic systems. Archive for Rational Mechanics and Analysis **20**, 120–152 (1965) https://doi.org/10.1007/BF00284614

[31] Krack, M., Gross, J.: Harmonic Balance for Nonlinear Vibration Problems. Mathematical Engineering. Springer, Cham (2019). https://doi.org/10.1007/978-3-030-14023-6

[32] Wiener, N.: The homogeneous chaos. American Journal of Mathematics **60**(4), 897–936 (1938) https://doi.org/10.2307/2371268

[33] Silverman, B.W.: Density Estimation for Statistics and Data Analysis. Chapman and Hall, London, New York (1986)

[34] Gradshteyn, I.S., Ryzhik, I.M.: Table of Integrals, Series, and Products, 7th edn. Academic Press, Amsterdam (2007)